

## Article

# Systematic Parameter Estimation and Dynamic Simulation of Cold Contact Fermentation for Alcohol-Free Beer Production

Dylan W. Pilarski and Dimitrios I. Gerogiorgis \* 

Institute for Materials and Processes (IMP), School of Engineering, University of Edinburgh, The King's Buildings, Edinburgh EH9 3FB, Scotland, UK

\* Correspondence: D.Gerogiorgis@ed.ac.uk; Tel.: +44-131-651-7072

**Abstract:** Global demand for Low-Alcohol Beer (LAB) and Alcohol-Free Beer (AFB) has surged due to flavor attributes, health benefits, and lifestyle changes, prompting efforts for process intensification. This paper aims to offer a detailed modelling basis for LAB manufacturing study and optimisation. A first-principles dynamic model for conventional beer manufacturing has been re-parameterized and used for dynamic simulation of Cold Contact Fermentation (CCF), an effective LAB and AFB production method, with concentrations tracked along plausible temperature manipulation profiles. Parameter estimation is pursued using industrial production data, with a detailed local sensitivity analysis portraying the effect of key parameter variation on sugar consumption, ethanol production, and key flavor component (ethyl acetate and diacetyl) evolution during (and final values after) CCF. Ethyl acetate (esters in general) affecting fruity flavors emerge as most sensitive to CCF conditions.

**Keywords:** beer; cold contact fermentation (CCF); parameter estimation; dynamic simulation



**Citation:** Pilarski, D.W.; Gerogiorgis, D.I. Systematic Parameter Estimation and Dynamic Simulation of Cold Contact Fermentation for Alcohol-Free Beer Production. *Processes* **2022**, *10*, 2400. <https://doi.org/10.3390/pr10112400>

Academic Editor: Anet Režek Jambak

Received: 3 July 2022

Accepted: 15 August 2022

Published: 15 November 2022

**Publisher's Note:** MDPI stays neutral with regard to jurisdictional claims in published maps and institutional affiliations.



**Copyright:** © 2022 by the authors. Licensee MDPI, Basel, Switzerland. This article is an open access article distributed under the terms and conditions of the Creative Commons Attribution (CC BY) license (<https://creativecommons.org/licenses/by/4.0/>).

## 1. Introduction

### 1.1. Low-Alcohol Beer (LAB) and Alcohol-Free Beer (AFB)

Beer brewing is an ancient practice [1], ingrained in local traditions of many cultures worldwide. Though resulting from agricultural village surpluses, the modern brewing industry has expanded its manufacturing and commercial presence to meet vast global consumption [2]: recent estimates by the World Health Organization (WHO, 2014) confirm that beer is the second most imbibed (top alcoholic) beverage worldwide [3]. This gradual progression from rural artisanal activity to modern industrial complex is illustrated by global production metrics, with  $1.95 \cdot 10^{11}$  L of beer produced in 2017 [4]. From a processing viewpoint, grouping beverages under the term 'beer' is a deliberate simplification, as it encompasses a multitude of different products of varying alcohol content [5], from Pilsners and Lagers (known as "bottom fermenting") to Weissbiers and Ales (known as "top fermenting") [6]. Different classifications and models [7] are based on alcohol strength (i.e., concentration). The range starts from Alcohol-Free Beer (AFB) at 0–1.2% (*v/v*) and moves to Low-Alcohol Beer (LAB) at 1.2–3% (*v/v*) before the classification of the vast majority of standard brew concentrations of 3–6% (*v/v*) [8,9].

The classification of AFB and LAB has a remarkable historical backdrop, with origins in the United States Prohibition era (1919–1933), but also as a reaction to raw material shortages during World War I and II (1939–1945) [9]. Global demand for zero-/low-alcohol products has surged recently, with an estimated 80% consumption increase from 2007 to 2012, in which it reached  $2.2 \cdot 10^9$  L yr<sup>-1</sup> [10]. Several explanations from a social perspective have been presented for this clear trend in beer sales, including stringent legal restrictions on consumption and wider awareness of moderation benefits. Recent efforts by beverage corporations to penetrate countries and access markets in which alcohol consumption is forbidden for religious reasons also seems to have had a significant contribution [9]. Health benefits of increased AFB and LAB consumption in contrast to standard alcoholic

beverages are substantial, as beneficial beer (antioxidant, anti-cancer, and phytoestrogen) components are retained at remarkably lower energy content (e.g., LAB has a 60.7% lower calorie content vs. pale ale) [11,12].

This differentiation among beer types is also critical in the different processing methods required to achieve different flavor profiles and strengths: even within the narrow AFB ethanol concentration, various production methods exist, categorized as either *physical* (post-processing) or *biological* (pre-processing) [8]. The former focus on dealcoholization via, e.g., distillation, adsorption, or dialysis: they require additional capital expenditure, being more expensive at production scale [10,13]. The latter alter the fermentation step itself via special yeast strains, yeast immobilization, CCF, or arrested fermentation, resulting in published ethanol concentration ranges from 0.02% (*v/v*) and up [11–15].

The most promising of these methods is Cold Contact Fermentation (CCF), also known as Cold Contact Process (CCP), which combines low fermentation temperatures (0–8 °C) and contact times of 24–100 h [16–19]. First proposed by Schur in 1983 [16], this batch method enjoys wide industrial use towards high AFB volumes [17,18]. Nevertheless, it may induce flavor deficiencies due to high levels of undesirable compounds, e.g., methional and Strecker aldehydes (2- and 3-methylbutanal) [17–19].

Laboratory-scale CCF research has been covered in the literature since inception [8,9], but CCF dynamic modeling has not yet received interest commensurate with beverage demand, especially compared with dynamic modeling and optimization success for ‘warmer’ ale and lager (6–22 °C) brewing [20–24]. We thus aim to pave the way for robust modeling platforms and higher industrial process efficiency.

Increased market LAB/AFB demand and health benefits vs. higher-alcohol beer are key drivers. This paper aims to establish a CCF modeling basis for process intensification as experimental work in the beer industry incurs high costs and implies use of process equipment for (risky) manipulations.

The latter may arise from the need for introducing new products (e.g., LAB/AFB), or implementing process improvements for existing products. This opportunity cost increases with production scale, as bigger plant facilities use larger equipment and thus incur a higher subsumed downtime cost. Revenue (thus, profit) to be maximized is a function of product sales, but engineering upgrades can have a critical effect on throughput. Evaluation of improvements via computational methods (e.g., process modeling) holds value for CCF, especially in light of increased global LAB/AFB consumption. Our goal is to probe CCF process potential using model reparameterization and sensitivity analyses.

## 1.2. Beer Manufacturing

Detailed understanding of beer manufacturing process steps (Figure 1) is key for appreciating how fermentation variants/specifications (e.g., CCF vs. warm fermentation) induce vast upstream and downstream changes in the seemingly simple interplay of barley malt, hops, yeast, and water [25].

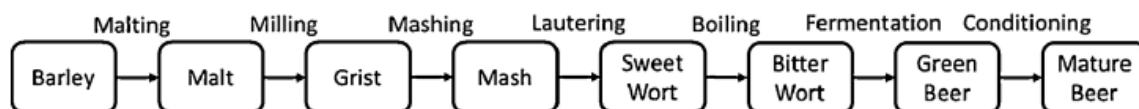


**Figure 1.** Block flow diagram illustrating material states and stages of a beer manufacturing process [20].

Beer manufacturing starts with the malting process: barley is converted to malt by kernel wetting and induced sprouting, simulating natural grain germination. The germinated embryo here secretes natural plant hormones (gibberellins) inducing production and activation of key enzymes (especially amylases) which are crucial towards hydrolyzing the endosperm starch later, during mashing [12]. Malt kilning to remove water follows, before degermination and storage until actual brewing use [5].

The brewing process commences with milling: the malt mixture is comminuted to grist, and the latter is added to water and mashed under heating, towards starch liquefaction and saccharification. The mash is then fed into the lauter tun, to separate the liquid wort from spent grist solids: this is the ‘first wort’ extraction, followed by subsequent extractions (‘last runnings’) of inferior composition. The liquid wort is transferred to a kettle and boiled to kill bacteria, remove dimethyl sulfide (DMS), induce flavor and color formation (Maillard melanoidin production), and cause enzyme degradation. This opportune point also serves secondary feed (hops, corn syrup) addition, as per brand recipes; wort boiling ensures isomerisation of hop alpha acids, as 99% of beers are brewed with hops [5]. The mixture is subsequently transferred to a whirlpool for precipitated hop and protein (‘hot trub’) removal, then to a cooling heat exchanger (as low as 0–1 °C for CCF) before fermentation [2,8].

The bitter, cooled wort from the boiling process is fed to fermentors with yeast (‘pitching’) and a small amount of air to promote initial biomass growth [25] and subsequent fermentable sugar consumption by yeast towards the production of beer, the very purpose of a fermentation phase [5]. Temperature and batch duration are pivotal, as they govern hundreds of chemical reactions and kinetics, driving flavor creation [26]. For the various cases for producing alcoholic beer via warm fermentation, temperatures range from 6 to 22 °C and total contact period of 5–21 days. The CCF method employs contact times of 24–100 h at temperatures of 0–8 °C, to inhibit ethanol formation while maintaining adequate flavor component formation levels. The resulting ‘green beer’ is washed by CO<sub>2</sub> bubbling to remove aldehydes before maturation and storage in casks, barrels, or bottles [1,2].

### 1.3. Organoleptic Constituents and Sensory Characteristics

Beer flavor is broader than taste, as the sum of perceptions from sensory element stimulation at the entrance of alimentary and respiratory tracts [25] also includes odor, aroma, and mouthfeel [26]. Key AFB batch flavor (quality) metrics include ethanol, pH, and residual (unfermented) sugar levels. However, an AFB deficiency is associated with excessive sweetness, worty off-flavors, bitterness, and possible absence of desirable aroma [27]. Chemical complexity thus poses further complications, as even acceptable physicochemical properties do not always imply satisfactory product taste [28]. Flavor is also perplexed by synergistic or suppressive phenomena due to other compounds: a mixture of, e.g., two or more aldehydes (all below thresholds) can still have a perceivable flavor effect [29,30].

Chief chemicals inducing undesirable beer flavor include Vicinal Diketones (VDKs), e.g., diacetyl (2,3-butanedione) and 2,3-pentanedione [31]. Other aldehydes are also crucial, e.g., 2-methylbutanal, 3-methylbutanal, furfural, acetaldehyde, isobutyraldehyde, 2-phenylacetaldehyde, methional, and 3-methylthiopropionaldehyde [32]. Worty off-flavors emerging from CCF are due to 2-methylbutanal, 3-methylbutanal, and 3-methylthiopropionaldehyde [17–19]. Higher (fusel) alcohol (e.g., propanol, butanol) levels must also be controlled, because their high concentration is strongly correlated with hangover effects. Esters ensure desirable beer flavor profiles (e.g., fruitiness): ethyl acetate, ethyl caproate, isoamyl acetate, ethyl caprylate, ethyl hexanoate, and phenyl ethyl acetate are critical [33].

### 1.4. Metabolic and Non-Metabolic Pathways

Several different types of yeast are used in beer brewing, though the most popular genus across all methods is *Saccharomyces*, with strains such as *Saccharomyces pastorianus* (formerly *Saccharomyces carlsbergensis*) and *Saccharomyces cerevisiae* (brewer’s yeast) mostly cited for CCF processing [34,35]. The most important reaction occurring over the course of any fermentation process is the conversion of the sugars in wort to ethanol and carbon dioxide. This is represented by the Gay-Lussac equation:



The reaction is overall exothermic, as clearly denoted by the negative sign of reaction enthalpy. Equation (1) is a clear simplification that does not portray the complex phenomena

during the fermentation process: these are distinguished into *metabolic* (intracellular) and *non-metabolic* (extracellular) [13]. Figure 2 presents a high-level overview of significant metabolic phenomena during beer fermentation.

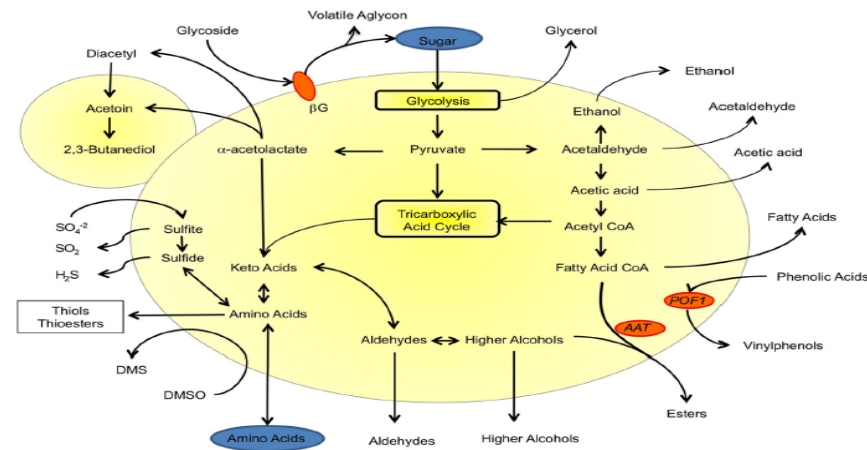


**Figure 2.** Metabolic pathway features of *Saccharomyces* strains affecting beer flavor and quality [35].

Carbonyls are formed via metabolic pathways (e.g., Strecker aldehyde degradation of amino acids, and lipid degradation), as well as by the non-metabolic pathway of Maillard reactions, which yield a vast variety of products [36,37]. Furfural (one of the principal products formed therein) can be used as a heating load indicator for beer at various process stages, as its concentration increases throughout brewing and through maturation [29]. Esters are produced in part by the transesterification of acetyl-coenzyme A and are tightly linked to lipid metabolism (Figure 2) [33,36]. Many pathways are inter-connected (e.g., Maillard reactions generate  $\alpha$ -dicarbonyls, while Strecker degradation consume them), showcasing the complexity of this challenging biochemical system vs. industrial manipulation goals.

## 2. Methodology

### 2.1. Mathematical Modeling of Fermentation

Beer fermentation is both nonlinear and complex, with its modeling and simulation described as a time-consuming task [2,20–24,31,38–40]. Though several mechanisms for enzyme activity exist, Michaelis–Menten and Monod kinetics are the most useful in the present effort. Michaelis–Menten kinetics represent the formation of a product ( $P_r$ ) resulting from the enzymatic ( $E$ ) linking with a substrate ( $S_r$ ), through the reversible formation of an intermediate ( $SE$ ), as per the following reactions:



Here,  $k_b$  and  $k_c$  represent the rate constant for the corresponding forward reactions at each step and  $k_a$  denotes the reverse reaction rate constant. The rate of product formation,  $r_p$ , is expressed as a ratio:

$$r_p = \frac{k_c C_S C_{ENZ}^0}{K_M + C_S} \quad (3)$$

where  $C_S$  and  $C_{ENZ}^0$  mark substrate and initial enzyme concentrations, respectively. The variable  $K_M$  is the Michaelis–Menten constant  $= k_a/k_b$ . While enzymes are chemical

substances produced by yeast to catalyze chemical reactions, biomass evolution itself can be described by the Monod equation:

$$r = \frac{r_m C_S}{k_{SS} + C_S} \quad (4)$$

where  $r$  is the specific biomass growth rate,  $r_m$  is its maximum value, and  $k_{SS}$  is the Monod constant.

Beer fermentation process modeling with explicit kinetics only emerged a few decades ago, rapidly gaining attention after the pioneering computational study of Engasser et al. in 1981 [38]. Process simulation efforts have however not been extended to CCF, with most experimental work at laboratory scale [9]. A chronological review of notable peer-reviewed advances on beer fermentation experiments, modeling, simulation, and optimization since 1981 was recently published [40].

## 2.2. Model Description

The de Andrés-Toro et al. model considers five state variables: sugar concentration ( $C_S$ ), ethanol concentration ( $C_E$ ), total suspended biomass concentration ( $X_S$ ), ethyl acetate concentration ( $C_{EA}$ ), and diacetyl concentration ( $C_{DY}$ ) [41]. The total biomass in a fermentation system comprises three entities, active ( $X_A$ ), latent/lag ( $X_L$ ), and dead ( $X_D$ ) biomass, without conservation constraints. Parameters were estimated from concentration trajectories obtained via several isothermal experiments performed at  $T = 8, 12, 16, 20,$  and  $24$  °C, using wort and yeast from Cruzcampo Breweries (Madrid, Spain) [41,42]. Beer fermentation is therein divided in two consecutive (lag and actual fermentation) phases. At the onset of brewing, there is no fermentation. During the lag phase, only dead cell settling and lag cell activation occurs: once the latter reaches 80%, both cell growth and fermentation commence. Thereafter, all four phenomena (settling, activation, growth, and fermentation) occur simultaneously until completion, followed by dilution, fresh ('green') beer maturation, and final packaging (Figure 3).

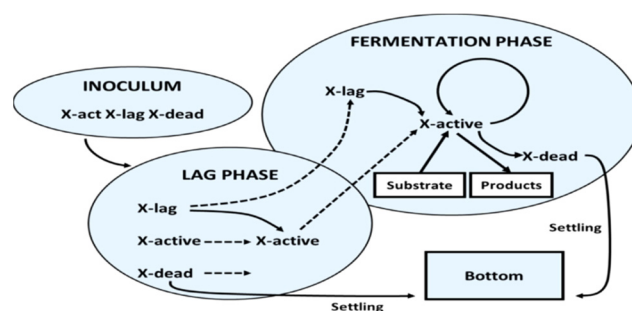


**Figure 3.** Fermentation lag and active phases as conceptually distinguished by de Andrés-Toro et al. [41].

The transition from lag to active cells is implicit in the model and does not require the addition of a secondary model operation (no explicit additional 'switch' is included in code implementation). Fermentation can be represented via DAE or ODEs differential equations governing sugar consumption, biomass and ethanol production, and flavor components formation as well as the corresponding Arrhenius expression linked to each of these component specific rates. All these equations are either a function of fermenter temperature ( $T$ ), fermentation time ( $t$ ), or both variables.

Experiments by de Andrés-Toro et al. allowed determination of the proportions of each type of cell in the fermenter. Though typically observed as lower in industrial breweries than represented in this model, the proportion of dead cells in the inoculum ( $X_{inc}$ ) was 50%,

while the remaining 50% of the inoculum comprises 48% lag cells and 2% active cells. This yeast mass balance can be written as:

$$0.02X_{\text{inc}} + 0.48X_{\text{inc}} = X_{\text{D}}(t = 0) = 0.5X_{\text{inc}} \quad (5)$$

where  $0.02X_{\text{inc}}$  is the proportion of active cells,  $X_{\text{A}}$ , in the inoculum and  $0.48X_{\text{inc}}$  is the proportion of lag cells in the inoculum,  $X_{\text{L}}$ . After the initial inoculation, the yeast,  $X_{\text{S}}$ , is suspended in the wort; the time-dependent biomass concentration comprises all (lag, active and dead) cells. This is denoted as:

$$X_{\text{S}}(t) = X_{\text{A}}(t) + X_{\text{L}}(t) + X_{\text{D}}(t) \quad (6)$$

The rate of conversion of lag cells to active cells is also considered in the model according to:

$$\frac{dX_{\text{L}}}{dt} = -\mu_{\text{L}}X_{\text{L}} \quad (7)$$

where  $\mu_{\text{L}}$  is the specific rate of lag cell activation, an Arrhenius-type exponential of temperature [41].

Active cells do not multiply in fermentation, but come from cell activation from the lag phase:

$$\frac{dX_{\text{A}}}{dt} = -\frac{dX_{\text{L}}}{dt}, t < t_{\text{L}} \quad (8)$$

where  $t_{\text{L}}$  is the duration of the fermentation lag phase, in which no cell deterioration is not considered.

Cell death occurs as expired cells settle out of the suspension to the vessel bottom, according to:

$$\frac{dX_{\text{D}}}{dt} = \mu_{\text{SD}}, t < t_{\text{L}} \quad (9)$$

where  $\mu_{\text{SD}}$  is the dead cell settling rate, a function of both fermentation temperature and duration. The rate of cell suspension is proportional to the dead cell concentration rate of change, according to:

$$\frac{dX_{\text{S}}}{dt} = -\frac{dX_{\text{D}}}{dt} \quad (10)$$

Dead cells settle, thus continuously removed from active cells in the fermentation broth according to:

$$\frac{dX_{\text{S}}}{dt} = \mu_{\text{x}} \cdot X_{\text{A}} - \mu_{\text{SD}} \cdot X_{\text{D}}, t \geq t_{\text{L}} \quad (11)$$

where  $\mu_{\text{x}}$  is the specific cell growth rate. Active cell concentration is governed by three distinct contributions for active cell growth, active cell death and latent (lag) cell activation, according to:

$$\frac{dX_{\text{A}}}{dt} = \mu_{\text{x}} \cdot X_{\text{A}} - \mu_{\text{DT}} \cdot X_{\text{A}} + \mu_{\text{L}} \cdot X_{\text{L}}, t \geq t_{\text{L}} \quad (12)$$

where  $\mu_{\text{DT}}$  is the specific cell death rate. Biomass activity and availability drives fermentation success, so Equation (12) links cell growth, activation, and death state variables and rates clearly throughout a batch.

Cell death, aside of Equations (10) and (11), is a function of dead cell settling and active cell death, according to:

$$\frac{dX_{\text{D}}}{dt} = -\mu_{\text{SD}} \cdot X_{\text{D}} + \mu_{\text{DT}} \cdot X_{\text{A}}, t \geq t_{\text{L}} \quad (13)$$

Substrate (sugar) consumption is considered proportional to active cell concentration, according to:

$$\frac{dC_{\text{S}}}{dt} = -\mu_{\text{S}} \cdot X_{\text{A}} \quad (14)$$

where  $\mu_S$  is the specific substrate consumption rate. The rate of change in sugar concentration in the fermenter is a function of sugar consumption by the active biomass. Ethanol formation is also a key component of this system, also considered proportional to active cell concentration, according to:

$$\frac{dC_E}{dt} = f_{\text{inhib}} \cdot \mu_E \cdot X_A \quad (15)$$

where  $f_{\text{inhib}}$  denotes the inhibition factor, portraying the detrimental effect of high ethanol concentrations on biomass (yeast) proliferation ( $\mu_E$  is the specific ethanol production rate). The biomass hence reacts to reduce the production of ethanol and promote cell longevity, according to:

$$f_{\text{inhib}} = 1 - \frac{C_E}{0.5C_{S0}} \quad (16)$$

where  $C_{S0}$  is the initial sugar concentration in the fermenter. Secondary flavor components are produced and consumed throughout the fermentation cycle. Among these components are esters, such as ethyl acetate, which is formed proportional to the active cell concentration according to:

$$\frac{dC_{EA}}{dt} = Y_{EA} \cdot \mu_x \cdot X_A \quad (17)$$

where  $Y_{EA}$  is the stoichiometric coefficient associated with the formation of ethyl acetate. Finally, diacetyl represents the overall composition of VDKs in the fermenter mixture. Here, the constants  $\mu_{DY}$  and  $\mu_{AB}$  are separate parameters describing the formation and reduction in diacetyl, respectively.

$$\frac{dC_{DY}}{dt} = \mu_{DY} \cdot C_S \cdot X_A - \mu_{AB} \cdot C_{DY} \cdot C_E \quad (18)$$

This equation represents specific substrate consumption rate in the Michaelis–Menten function form, particularly useful for yeast and enzyme kinetic expressions [41]. The specific growth rate depends on sugar concentration (wort density), but also on instantaneous ethanol concentration, according to:

$$\mu_x = \frac{\mu_{x0} \cdot C_S(t)}{k_x + C_E} \quad (19)$$

where  $k_x$  is the biomass affinity constant and  $\mu_{x0}$  is the maximum cell growth rate. The dead cell settling rate depends on initial sugar as well as instantaneous ethanol concentration, according to:

$$\mu_{SD} = \frac{0.5 \cdot \mu_{SD0} \cdot C_{S0}}{0.5 \cdot C_{S0} + C_E} \quad (20)$$

where  $\mu_{SD0}$  is the maximum dead cell settling rate. The specific substrate consumption rate once again depends on sugar concentration (but not on any other instantaneous concentration), according to:

$$\mu_S = \frac{\mu_{S0} \cdot C_S}{k_S + C_S} \quad (21)$$

where  $k_S$  is the substrate affinity constant and  $\mu_{S0}$  is the maximum sugar consumption rate. Moreover, the specific ethanol production rate is provided by a similar expression of identical form, according to:

$$\mu_e = \frac{\mu_{e0} \cdot C_S}{k_e + C_S} \quad (22)$$

where  $k_e$  is the ethanol affinity constant and  $\mu_{e0}$  is the maximum ethanol production rate (at the onset). All specific rate parameters obey Arrhenius-type expressions which are determined experimentally:

$$\mu_{i0} = \exp\left(A_i + \frac{B_i}{T}\right) \quad (23)$$

The format of Equation (23) has both parameters within the exponential, as per de Andrés-Toro data [41]. Corresponding ( $A_i$ ,  $B_i$ ) parameter coefficient values and literature sources are listed in Tables 1 and 2.

**Table 1.** Tabulated Arrhenius parameters ( $A_i$  and  $B_i$ ) [41].

| Rates + Factors | Description                             | $A_i$   | $B_i$      |
|-----------------|---|---------|------------|
| $\mu_{SD0}$     | Maximum dead cell settling rate         | 33.82   | −10,033.28 |
| $\mu_{X0}$      | Maximum cell growth rate                | 108.31  | −31,934.09 |
| $\mu_{S0}$      | Maximum sugar consumption rate          | −41.92  | 11,654.64  |
| $\mu_{e0}$      | Maximum ethanol production rate         | 3.27    | −1267.24   |
| $\mu_{DT}$      | Specific cell death rate                | 130.16  | −38,313.00 |
| $\mu_L$         | Specific cell activation rate           | 30.72   | −9501.54   |
| $k_e = k_S$     | Affinity constant for sugar and ethanol | −119.63 | 34,203.95  |
| $Y_{EA}$        | Stoichiometric factor—EA production     | 89.92   | −26,589.00 |

**Table 2.** Tabulated diacetyl production and consumption rate parameters [43].

| Rates      | Description                  | Value                   | Units                                  |
|------------|------------------------------|-------------------------|--|
| $\mu_{DY}$ | Rate of diacetyl production  | $1.27672 \cdot 10^{-4}$ | $\text{g}^{-1} \text{h}^{-1} \text{L}$ |
| $\mu_{AB}$ | Rate of diacetyl consumption | $1.13864 \cdot 10^{-3}$ | $\text{g}^{-1} \text{h}^{-1} \text{L}$ |

### 2.3. Numerical Integration

The de Andrés-Toro et al. model [41] is implemented in the MATLAB (R2018b) environment and integrated numerically via ode45: the code comprises 13 (11 differential and 1 algebraic) equations, one of which inputs the temperature profile to Arrhenius-type parameter definitions, Equation (23), at each time point. Initial conditions with source (or calculation method) are provided in Table 3.

**Table 3.** Initial condition values with origin (or calculation method), for dynamic simulation.

| Variable | Initial Condition ( $t = 0$ ) | Units                          | Literature Reference/Calculation                                       |
|----------|-------------------------------|--------------------------------|--|
| $X_L$    | 1.92                          | $\text{g} \cdot \text{L}^{-1}$ | $0.02X_{\text{inc}} + 0.48X_{\text{inc}} = X_D(0) = 0.5X_{\text{inc}}$ |
| $X_A$    | 0.08                          | $\text{g} \cdot \text{L}^{-1}$ | $0.02X_{\text{inc}} + 0.48X_{\text{inc}} = X_D(0) = 0.5X_{\text{inc}}$ |
| $X_D$    | 2.00                          | $\text{g} \cdot \text{L}^{-1}$ | $0.02X_{\text{inc}} + 0.48X_{\text{inc}} = X_D(0) = 0.5X_{\text{inc}}$ |
| $X_S$    | 4.00                          | $\text{g} \cdot \text{L}^{-1}$ | [41]   |
| $C_S$    | 130.00                        | $\text{g} \cdot \text{L}^{-1}$ | [41]   |
| $C_E$    | 0                             | $\text{g} \cdot \text{L}^{-1}$ | [41]   |
| $C_{EA}$ | 0                             | ppm                            | [41]   |
| $C_{DY}$ | 0                             | ppm                            | [41]   |
| $T$      | 286.15                        | K                              | Interpolation of temperature profile from [20]                         |

The absolute solver tolerance ( $10^{-9}$ ) ensures high precision as results from our validation trials serve as a foundation for comparative analyses vs. previous papers [20–22], confirmed as appropriate. This DAE system is relatively small and has an acceptably short total computation time of ca. 2 s. The default MATLAB solver (ode45) options are used on an Intel Core™ i7-7700HQ (2.80 GHz) CPU.

#### 2.4. Dynamic Simulation of Warm Fermentation for Code Validation

To ensure the foregoing mathematical model credibly describes fermentation systems, our script has been used to obtain several responses used for validation after comparison with published results.

The temperature profile for this model validation considers a single isothermal ( $T = 13\text{ }^{\circ}\text{C}$ ) profile incorporated into the model as an interpolation from  $t_0 = 0$  to  $t_f = 160$  h with both initial and final fermentation temperature values at  $T = 286.15$  K. The numerical integration time step employed was  $\Delta t = 1$  h throughout; we also confirmed that a shorter time step does not improve accuracy.

The temperature profile is critical to the entire model as it governs Arrhenius expressions and therefore determines the magnitudes of each model parameter per unit time, which in turn guides the dynamics of the entire system. At each time node, the parameters are solved for and incorporated into the DAE system, and numerical integration provides results for all response trajectories (Figure 4).

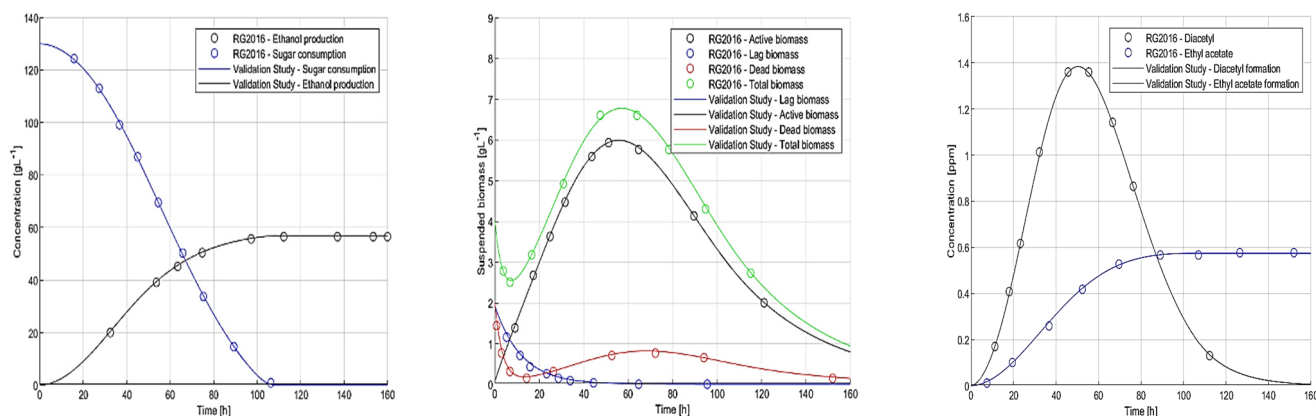


**Figure 4.** Sugar, biomass, and ethanol concentration responses: warm fermentation simulations,  $T = 13\text{ }^{\circ}\text{C}$ . Discrete points represent results published in literature (RG2016) for code validation purposes [20].

Our simulations yield sugar and ethanol concentration responses throughout this fermentation ( $T = 13\text{ }^{\circ}\text{C} = 286.15$  K), for MATLAB code validation purposes vs. our earlier (2016) publication [20].

Figure 4 shows that fermented sugar concentration starts at  $130\text{ g L}^{-1}$ , decreasing until completely consumed after 106 h of fermentation, a value coinciding with theoretical (complete) sugar depletion. Ethanol concentration in the fermenter begins at 0 and increases over the duration of the fermentation process until 106 h, after which point no more is produced until the fermentation ends ( $t = 160$  h).

The total suspended biomass is the sum of active, lag, and dead biomass in the fermenter: lag cells decrease from the start until  $t = 65$  h, from when no lag cells are further present in the fermenter. Active cells in the fermenter increase relatively quickly at first, reaching their highest concentration at  $t = 56$  h until they then decrease again throughout the remainder of the fermentation process. Dead cell concentration can be described as dropping precipitously relative to other biomass responses until  $t = 14$  h, before rebounding and increasing until  $t = 70$  h before finally decreasing steadily for the remainder of the fermentation process. The total biomass signal (green line) is the sum of all three responses per unit time and features a minimum (before  $t = 10$  h) and a maximum (about  $t = 60$  h).

Ethyl acetate and diacetyl responses (initial condition: 0 ppm) evolve over fermentation (Figure 4). Diacetyl increases at a high rate, peaking at  $t = 50$  h and tailing off for the rest of the fermentation. Ethyl acetate also increases albeit at a much slower rate, it peaks at  $t = 106$  h (as the ethanol signal) and remains constant thereafter, since sugar (as per concentration signal) is fully consumed at this point.

### 3. Industrial Processing and Experimental Results

#### 3.1. Process Description

An industrial fermentation for a commercial (0.5% ABV) beer product was performed under CCF conditions, employing an actual batch volume of  $V = 9.19 \cdot 10^4$  L in an industrial cylindrical fermenter of volume  $V = 2.00 \cdot 10^5$  L (slightly less than half-full) without any use of mechanical stirring. A standard gravity wort was subjected to *Saccharomyces pastorianus* yeast for this industrial CCF run (wort specifications are provided in Tables 4 and 6; high-gravity worts have SGs between 1.055 and 1.07). The exact CCF temperature profile was not provided, but varies between  $T = 5$  and  $6.5$  °C. Three separate temperature profiles were thus inferred as possibilities for investigation; an isothermal at  $T(t) = 5$  °C, another at  $T(t) = 6.5$  °C, and a linear profile increasing from  $T = 5$  to  $6.5$  °C over a time of  $t_{\text{span}} = 60$  h.

**Table 4.** Tabulated data from the industrial partner specifying the change in specific gravity (SG), acetaldehyde concentration (ppm) and pH vs. time (fermentation run duration) for a CCF experiment.

| Time (h)      | Specific Gravity (SG) | Acetaldehyde Concentration (ppm) | pH   |
|---------------|-----------------------|----------------------------------|------|
| 0             | 1.027                 | 0                                | 4.09 |
| 12            | 1.027                 | (-)                              | (-)  |
| 24            | 1.026                 | (-)                              | (-)  |
| 36            | 1.025                 | (-)                              | (-)  |
| 48            | 1.025                 | (-)                              | (-)  |
| 60            | 1.024                 | (-)                              | 4.07 |
| post-dilution | 1.015–1.016           | 24.50                            | (-)  |

Though other temperature profiles (especially nonlinear) may exist, extending the scope of the problem to probing all putative temperature profiles of interest within the provided industrial range is straightforward to implement if one modifies the bounds for this CCF process ( $5$  °C  $\leq T(t) \leq 6.5$  °C).

Following the completion of the said industrial CCF process, the initial batch was diluted using  $V = 5.55 \cdot 10^4$  L of water for a total post-dilution volume of  $V = 1.47 \cdot 10^5$  L. The final product was then evaluated as per internal procedures, including tasting by an expert flavor panel, along with additional sensory analyses via gas chromatography for the final packaged product ('final pack'). Details on experimental methods for CCF organic compound determination are provided in [2,5,25,35], with liquid/gas chromatographic methods (HPLC, GC-MS) often used for precision measurements.

The data received were categorized into two sets. The first group consists of responses that are not used in the previously validated de Andrés-Toro et al. model and the second group consists of data for responses used explicitly in the previously validated de Andrés-Toro et al. model (Table 4).

Dashes (-) in Tables 4 and 5 imply that no concentration data are available for these time points. Industrial data corresponding to alcohol content is usually provided and reported in the literature as units of Alcohol-by-Volume (ABV), defined as the number of  $\text{cm}^3$  ethanol per  $100 \text{ cm}^3$  beer or % ( $v/v$ ). Experimental analysis results which were essential in our study are tabulated in Table 5.

**Table 5.** Tabulated data specifying change in concentrations of ethyl acetate ( $C_{EA}$ ), diacetyl ( $C_{DY}$ ), ethanol ( $C_E$ ), ABV, total suspended biomass ( $X_S$ ), and sugar ( $C_S$ ) vs. time (fermentation run duration).

| Time (h)      | $C_{EA}$ (ppm) | $C_{DY}$ (ppm) | $C_E$ (g L <sup>-1</sup> ) | ABV (% $v/v$ ) | $X_S$ (cells·mL <sup>-1</sup> ) | $C_S$ (g·L <sup>-1</sup> ) |
|---------------|----------------|----------------|----------------------------|----------------|---------------------------------|----------------------------|
| 0             | 0              | 0              | 0                          | 0              | $3 \cdot 10^7$                  | 68.1                       |
| 12            | (-)            | (-)            | (-)                        | (-)            | (-)                             | (-)                        |
| 24            | (-)            | (-)            | (-)                        | (-)            | (-)                             | (-)                        |
| 36            | (-)            | (-)            | (-)                        | (-)            | (-)                             | (-)                        |
| 48            | (-)            | (-)            | (-)                        | (-)            | (-)                             | (-)                        |
| 60            | 5.60           | 0.032          | 3.80                       | 0.48           | (-)                             | 60.7                       |
| Post-dilution | 3.50           | 0.020          | 2.37                       | 0.30           | (-)                             | 38.2–40.8                  |

Tables 4 and 5 indicate that the data provided capture various measured concentrations of interest at the starting point ( $t = 0$ ), and at either the final and/or the post-dilution value, but not while fermentation evolves (sampling is laborious; offline analyses imply inherent drift and inaccuracy). Offline monitoring of sugars is possible via High Performance Liquid Chromatography (HPLC) [31].

### 3.2. Flavor Considerations

The composite flavor of beer obtained via CCF is complex, due to the presence of hundreds of flavor compounds [26]. Nevertheless, only total sugar, ethanol, diacetyl, and ethyl acetate were included as responses in the de Andrés-Toro et al. model [41], also employed exclusively in this paper. Thus, it is useful to compare industrial final concentration measurements against established flavor thresholds reported in the literature, to probe the importance of known flavor contributors (Table 6).

**Table 6.** Key flavor component concentrations vs. respective thresholds for a 0.5%  $v/v$  beer.

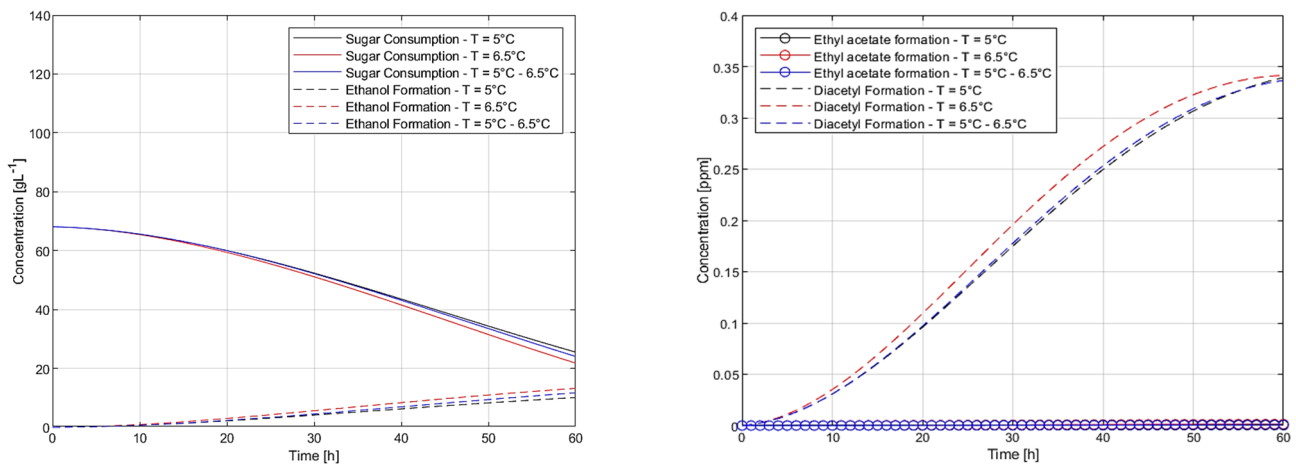
| Chemical Name       | Final Pack Concentration (ppm) | Flavor Threshold (ppm) | Ref. | Flavor Association              |
|---------------------|--------------------------------|------------------------|------|---------------------------------|
| Aldehydes (Non-VDK) |                                |                        |      |                                 |
| 2-methylbutanal     | $4.96 \cdot 10^{-3}$           | $1.00 \cdot 10^{-3}$   | [32] | Almond, apple-like, malty, wort |
| 3-methylbutanal     | $1.98 \cdot 10^{-2}$           | $5.60 \cdot 10^{-2}$   | [29] | Malty, chocolate, cherry, wort  |
| Furfural            | $1.12 \cdot 10^{-2}$           | $1.50 \cdot 10^1$      | [44] | Caramel, bread, cooked meat     |
| Trans-2-nonenal     | $4.00 \cdot 10^{-4}$           | $3.00 \cdot 10^{-5}$   | [29] | Cardboard, papery, cucumber     |
| Acetaldehyde        | $2.82 \cdot 10^{-3}$           | 1.10                   | [29] | Green apple, fruity             |
| VDKs                |                                |                        |      |                                 |
| Diacetyl            | $2.00 \cdot 10^{-2}$           | $1.50 \cdot 10^1$      | [45] | Buttery, butterscotch           |
| Pentane-2,3-dione   | $1.00 \cdot 10^{-2}$           | $9.00 \cdot 10^1$      | [45] | Buttery                         |
| Fusel alcohols      |                                |                        |      |                                 |
| Propanol            | 1.70                           | $6.00 \cdot 10^2$      | [46] | Solvent-like                    |
| Isobutanol          | 1.80                           | $1.00 \cdot 10^2$      | [46] | Solvent-like                    |
| Esters              |                                |                        |      |                                 |
| Ethyl hexanoate     | $1.00 \cdot 10^{-2}$           | $2.00 \cdot 10^{-1}$   | [23] | Apple, pineapple                |
| Isoamyl acetate     | $5.00 \cdot 10^{-2}$           | $5.00 \cdot 10^{-1}$   | [44] | Banana, pear                    |
| Ethyl acetate       | $9.00 \cdot 10^{-1}$           | $2.10 \cdot 10^1$      | [33] | Fruity, solvent-like            |

Table 6 shows that 2-methylbutanal and *trans*-2-nonenal were detected at concentrations higher than literature flavor thresholds; this is possibly a manifestation of ‘staling aldehyde’ effects. Surpassing a single flavor threshold does not necessarily have quantifiable sensory implications, given the complex nature of beer, and the possible synergistic or suppressive flavor effects [13,27]. Moreover, the literature flavor thresholds are obtained under controlled conditions (expert panels) and should be judiciously used in regard to pre- and post-dilution points (even more vs. maturation), also noting the fact that different consumer markets generally respond differently to different flavors. Developing a solid understanding of AFB maturation kinetics is critical to such flavor quantification.

## 4. Fermentation Response Comparisons

### 4.1. Initial Condition Considerations

The CCF initial conditions, stipulated temperature manipulation profiles and resulting final concentration measurements are significantly different from warm fermentation results (Section 2.4). To evaluate how the previously validated de Andrés-Toro et al. (Figure 4;  $T = 13$  °C) model functions with different CCF initial conditions (sugar concentration, fermentation duration, and  $T(t)$  profiles, as flavor compounds and ethanol are initially zero), several simulations were completed and plotted. Firstly, model response variations for sugar consumption and ethanol formation were assessed (Figure 5).



**Figure 5.** Sugar, ethanol, ethyl acetate, and diacetyl responses for three CCF temperature profiles.

Even for the lower initial sugar concentration, its complete depletion is not achieved: residual sugar remains after 60 h. Sugar concentration does not match the experimental values reported in Table 5:  $C_S(60\text{ h}) = 20$  vs.  $60.7\text{ g}\cdot\text{L}^{-1}$ . The use of three different temperature profiles produces a relative difference of 5.7% in the values of  $C_S(60\text{ h})$  between the lower and higher temperature isotherms. Ethanol production is significantly reduced under these (much colder temperature) conditions, and model results present it as much higher than the final concentration target of  $C_S(60\text{ h}) = 3.7872\text{ g}\cdot\text{L}^{-1}$ .

The three different temperature profiles induce a clear relative difference of 15.8% in  $C_E(60\text{ h})$  between lower and higher  $T(t)$  isotherms, indicating the  $T(t)$  profile has a stronger impact on ethanol formation vs. sugar consumption. All these findings imply a clear need for model reparameterization.

Diacetyl and ethyl acetate curves in CCF concentration range (0–0.4 ppm) are provided in Figure 5. Diacetyl formation proceeds faster for the warmest  $T(t)$  profile vs. the other two, but the final value variation for  $C_{DY}(60\text{ h})$  is miniscule (0.8%) between the lower and higher temperature isotherms. Ethyl acetate production is extremely limited in all three simulations ( $C_{EA} < 1.4\cdot 10^{-3}$  ppm), but for this by-product there is great  $C_{EA}(60\text{ h})$  variation (86%) between the lower and higher  $T(t)$  isotherms.

#### 4.2. Comparative Analysis

Current CCF simulations were compared with de Andrés-Toro et al. ( $T = 13\text{ }^\circ\text{C}$ ) model results via relative error analysis of state variables ( $\theta$ ). The Relative Percentage Error (*RPE*) is defined as:

$$RPE = 100 \left( \frac{\theta_{j,IC} - \theta_{j,dAT}(t)}{\theta_{j,dAT}(t)} \right) \quad (24)$$

where  $\theta_{j,IC}$  denote state variable values ( $t_{\text{span}} = 60\text{ h}$ ) from our init. cond. simulation, and  $\theta_{j,dAT}(t)$  is the final state variable value using the de Andrés-Toro et al. ( $T = 13\text{ }^\circ\text{C}$ ) model, for  $t_{\text{span}} = 160\text{ h}$  (Figure 6).

Figure 6a presents *RPE* results: negative values indicate final-time concentrations smaller than the de Andrés-Toro et al. model results for warm fermentation, with differences being clearly significant.

Figure 6b shows a logarithmic *RPE* scale for comparison of seven state (response) variables with enormous final-time model value differences between the two regimes, which span several orders of magnitude. Only the upper ( $T = 6.5\text{ }^\circ\text{C}$ ) and lower ( $T = 5\text{ }^\circ\text{C}$ ) temperature profiles are considered (CCF extremes). A higher temperature isotherm generally induces a larger (if not similar) *RPE* for all concentrations.

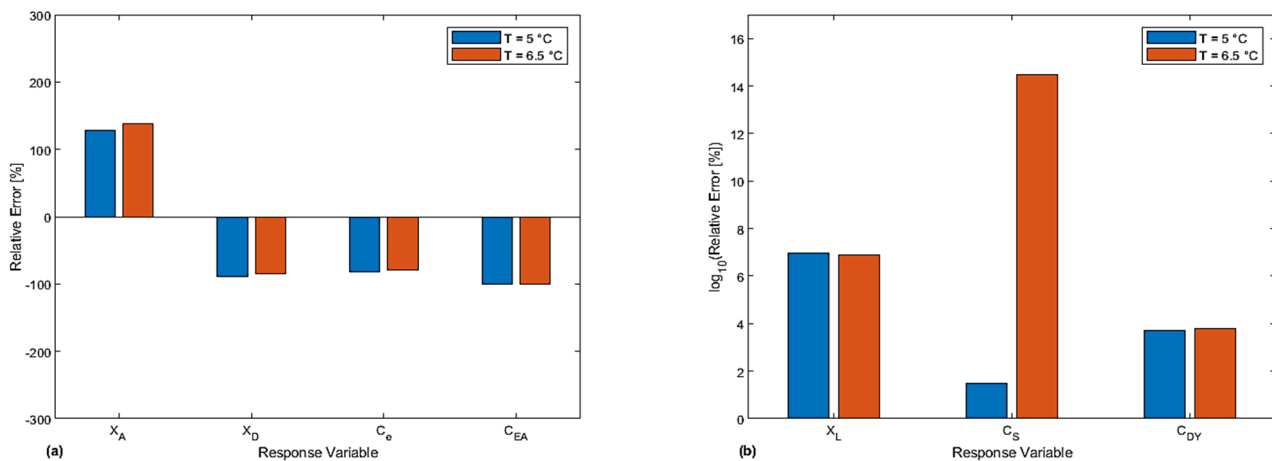


**Figure 6.** Model results comparison: (a)  $RPE$ , (b)  $\log_{10}RPE$ , for CCF/warm initial conditions ( $t_f = 60$  vs. 160 h).

Also,  $C_S$  has a very high  $RPE$  for the higher manipulation, but a much lower one for the lower  $T(t)$  manipulation. The remarkable  $RPE$  discrepancy for sugar concentration ( $C_S$ ) is a numerical artifact because of its near-complete consumption at final time in warm ( $T = 13\text{ }^\circ\text{C}$ ) but not in CCF (e.g., as seen in Figure 5).

The time horizon considered for dynamic simulations of CCF vs. warm fermentation (Figure 6) is a fair comparison basis in the sense that both processes are complete, but we also note that the span is very different (60 vs. 160 h). Therefore, additional model result comparisons were performed between CCF and warm fermentation initial conditions, this time for all values at  $t_{\text{span}} = 60$  h (Figure 7).

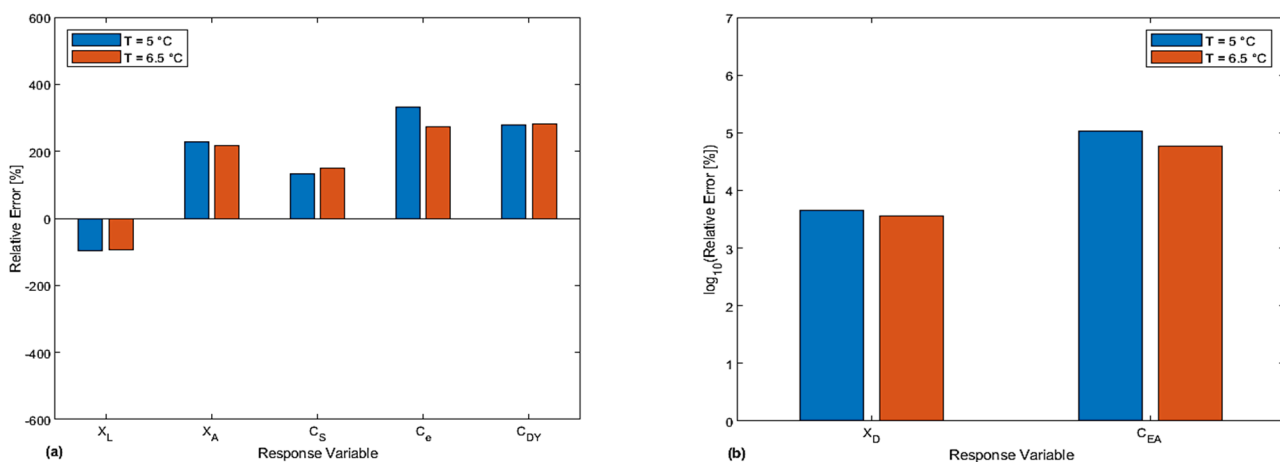


**Figure 7.** Model results comparison: (a)  $RPE$ , (b)  $\log_{10}RPE$ , for CCF/warm initial conditions, on par ( $t = 60$  h, both).

Figure 7a presents  $RPE$  results: this time the trend is reversed, with positive values indicating that the time point (and horizon) selected is pivotal (CCF completed, warm run in full swing at  $t = 60$  h). The operational asymmetry (complete vs. mid-time fermentation) is the reason  $RPE$  is higher here. Figure 7b has a logarithmic  $RPE$  scale to analyze dead cell ( $X_D$ ) and ethyl acetate ( $C_{EA}$ ) concentrations. Lower temperature isotherms produce a slightly larger (positive)  $RPE$  for all dynamic state variables, which is the exact reverse trend compared with that of Figure 6 (due to incomplete warm fermentation).

Sugar concentration  $RPE$  variations are most pronounced between Figures 6 and 7, but this is hardly surprising due to high (nonzero) initial ( $C_S$ ) values, and the very low ones upon brewing completion. Ethyl acetate has a very high  $RPE$  here (much higher

than Figure 6) because its production virtually plateaued as early as  $t = 60$  h at  $T = 13$  °C (Figure 4), but CCF has a much lower final  $C_{EA}$  value (Figure 5).

Model responses to any other  $T(t)$  profile between the two isothermal  $T(t) = 5$  and  $6.5$  °C cases (e.g., the linear upward profile between the two) hence do not need to be comprehensively enumerated. For all  $T(t)$  profiles in CCF range,  $C_{EA}(t)$  exhibits conspicuous departure from warm fermentation. Warm fermentation model [41] parameters are thus not reliable for CCF simulation: we note that CCF (low  $T$ ) seems to suppress undesirable by-product ( $C_{EA}$ ) while also reducing alcohol ( $C_E$ ) generation.

Figure 5 model results grossly underestimate  $C_{EA}$  and overestimate  $C_E$  values vs. experiments (Table 5). Though trends are broadly correct, all discrepancies highlight the need for model reparameterization; therein, we only used CCF (without ‘warm’ run) data, to avoid outlier effects and artificial uncertainty.

## 5. Parameter Estimation

### 5.1. Background

To minimize discrepancies, parameterization of the de Andrés-Toro et al. model for CCF + initial conditions was performed. This parameterization entailed determining a new set of model parameters so that final CCF target responses match experimental data via error minimization:

$$\min_{\theta_i} J(\theta_i) \quad (25)$$

where  $J$  is the objective function to be minimized and  $\theta_i$  is the model response used in minimization. Given the nonlinear dynamic model, an algorithm is required in order to determine a set of parameters ( $x_i$ ) in a systematic, efficient way. This was performed in MATLAB to minimize the value of least-squares regression between CCF model target responses and experimental data using the Nelder–Mead simplex method (MATLAB’s `fminsearch`) with tolerances of  $1 \cdot 10^{-4}$  on both decision variables and objective function. An outline of the algorithm and MATLAB code is shown in Figure 8. The Nelder–Mead algorithm is a simplex-based direct search method for nonlinear optimization, minimizing a function of  $N$  variables by comparing its values at the  $N + 1$  vertices of a simplex, replacing the highest-value vertex by another point, eventually converging to the minimum [47]. Successive replacements occur via three different operations (reflection, contraction, and expansion).

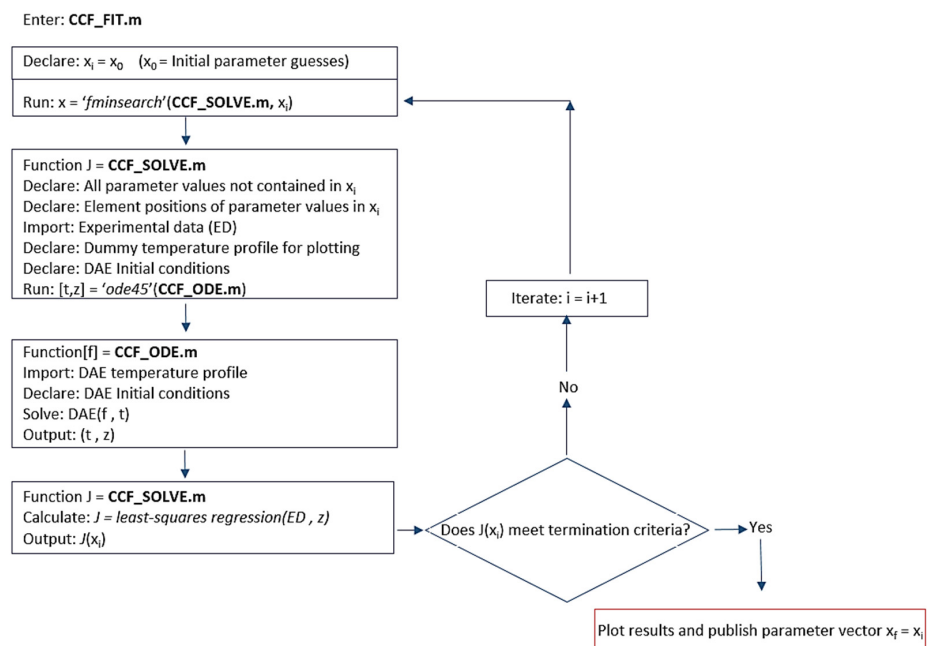


Figure 8. High-level flow diagram of MATLAB code for CCF model parameterization.

The least-squares regression (Figure 8) as  $J$  is the objective function and formalized generally as:

$$J = \sum_{i=1}^N (\theta_{i,\text{measured}} - \theta_{i,\text{model}})^2 \quad (26)$$

The variance-weighted least-squares regression ( $J_{\text{VAR}}$ ) considers a multiplier in the objective:

$$J_{\text{VAR}} = \sum_{i=1}^N \frac{1}{S_{i\theta}^2} (\theta_{i,\text{measured}} - \theta_{i,\text{model}})^2 \quad (27)$$

where  $S_{i\theta}^2$  is the variance according to:

$$S_{i\theta}^2 = \frac{1}{N-1} \sum_{i=1}^N |\theta_{i,\text{measured}} - \bar{\theta}_{i,\text{measured}}|^2 \quad (28)$$

where  $(N-1)$  the degrees of freedom and  $\bar{\theta}_i$  is arithmetic mean (average). Due to industrial data availability limitations, response variance weighting provided no additional statistical benefit over the standard least-squares regression model (1–2 data points require matching per target response).

A reparameterization solution is achieved by variation in the initial guess vector ( $x_0$ ) which originally consists of warm fermentation parameter values previously reported in the literature [41]. Convergence requires substantial (>80%) variation in three or more of the target parameter guesses in the correct direction of minimization (e.g.,  $A_{\text{YEA}}$ ,  $\mu_{\text{DY}}$ ,  $A_{\mu\text{e}0}$ ), for the reparameterization to be achieved converge within the same number of iterations required by the standard least-squares regression. Non-weighted least-squares regression was used, in the interest of computational efficiency. Weighted least-squares regression may be more advantageous with larger experimental campaigns, due to its power in handling heterogeneous datasets of varying size and possible uncertainty [48–50].

## 5.2. Model Reparameterization Trials

Selecting parameters and numerical values was a key stage of our reparameterization trials. The twelve parameters included in the MATLAB estimation vector ( $x_0$ ) and varying as unconstrained in the least-squares regression procedure are:  $A_{\mu\text{e}0}$ ,  $B_{\mu\text{e}0}$ ,  $B_{\mu\text{S}0}$ ,  $A_{\text{kes}}$ ,  $B_{\text{kes}}$ ,  $A_{\mu\text{X}0}$ ,  $B_{\mu\text{X}0}$ ,  $A_{\text{YEA}}$ ,  $B_{\text{YEA}}$ ,  $\mu_{\text{AB}}$ , and  $\mu_{\text{DY}}$ . The six parameters which are not included in the said vector ( $x_0$ ) are:  $A_{\mu\text{SD}0}$ ,  $B_{\mu\text{SD}0}$ ,  $A_{\mu\text{DT}}$ ,  $B_{\mu\text{DT}}$ ,  $A_{\mu\text{L}}$ , and  $B_{\mu\text{L}}$ . A series of trials consider various parameter subsets, to converge to a parameter solution ( $x_0^*$ ) which achieves convergence for the non-fixed components, satisfying initial and final-time data (Table 5).

Beyond Trials 1–2 and the severe non-convergence issues identified, subsequent efforts sought to converge to a credible parameter estimation by first establishing the minimum subset of  $x_0$  components which allow for convergence (Trial 3) and then adding, subtracting, or alternating parameter pairs based on previous trial performance to achieve converging  $x_0$  subsets (Trial 4–8). Once such a parameter vector subset was identified (Trials 9–13), the approach was continued with one-at-a-time changes, to see if and how convergence may be affected by such single substitutions. This approach yields converged solutions without exhaustive enumeration of all possible  $x_0$  subsets, saving CPU expense. Our aim is not the full list of all converged  $x_0$  subsets (these would be prohibitively numerous, because Table 5 data offer very few constraints), but a converged  $x_0$  subset with the minimum norm transition from the original (de Andrés-Toro et al.) parameter values [41].

Table 7 presents the 17 separate cases analyzed, each entailing model parameters computation for each of the three postulated  $T(t)$  profiles. A total of 51 trials were conducted with corresponding convergence, iteration, and parameter values recorded. For example, Trial 11 ( $T = 5\text{--}6.5$  °C) required 621 iterations and 1029 function evaluations: this is relatively quick compared with several other cases (e.g., Trial 16: 990 iterations; 1586 function evaluations). Trials resulting in slight non-convergence lasted longer than those achieving full convergence; CPU time ranged between 4 min and 2 h.

**Table 7.** The 17 parameterization trials: parameters computed in each trial (✓) vs. fixed ones (–), and corresponding convergence behavior. ‘Severe’ and ‘slight’ non-convergence indicate problems with multiple or only one response variable vs. final-time industrial data, respectively. Trial 11 yields the final result. The symbol \* denotes that (unconstrained) biomass responses exhibit unrealistic behavior.

| Trial | $A_{\mu e0}$ | $B_{\mu e0}$ | $A_{\mu S0}$ | $B_{\mu S0}$ | $A_{kes}$ | $B_{kes}$ | $A_{\mu X0}$ | $B_{\mu X0}$ | $A_{YEA}$ | $B_{YEA}$ | $\mu_{AB}$ | $\mu_{DY}$ | Result                 |
|-------|--------------|--------------|--------------|--------------|-----------|-----------|--------------|--------------|-----------|-----------|------------|------------|------------------------|
| 1     | ✓            | ✓            | ✓            | ✓            | ✓         | ✓         | ✓            | ✓            | ✓         | ✓         | ✓          | ✓          | Severe Non-Convergence |
| 2     | ✓            | ✓            | ✓            | ✓            | ✓         | ✓         | ✓            | ✓            | ✓         | ✓         | (–)        | ✓          | Severe Non-Convergence |
| 3     | (–)          | (–)          | (–)          | (–)          | ✓         | (–)       | ✓            | (–)          | (–)       | (–)       | (–)        | ✓          | Slight Non-Convergence |
| 4     | (–)          | (–)          | (–)          | (–)          | ✓         | (–)       | ✓            | ✓            | (–)       | (–)       | (–)        | ✓          | Slight Non-Convergence |
| 5     | (–)          | (–)          | (–)          | ✓            | ✓         | (–)       | ✓            | (–)          | (–)       | (–)       | (–)        | ✓          | Convergence            |
| 6     | (–)          | ✓            | (–)          | ✓            | ✓         | (–)       | ✓            | (–)          | (–)       | (–)       | (–)        | ✓          | Slight Non-Convergence |
| 7     | (–)          | ✓            | (–)          | ✓            | ✓         | (–)       | ✓            | (–)          | ✓         | (–)       | ✓          | (–)        | Slight Non-Convergence |
| 8     | (–)          | ✓            | (–)          | ✓            | ✓         | (–)       | ✓            | (–)          | (–)       | ✓         | ✓          | (–)        | Slight Non-Convergence |
| 9     | (–)          | ✓            | (–)          | ✓            | ✓         | (–)       | (–)          | ✓            | ✓         | (–)       | (–)        | ✓          | Convergence            |
| 10    | (–)          | ✓            | ✓            | (–)          | (–)       | ✓         | ✓            | (–)          | ✓         | (–)       | (–)        | ✓          | Convergence            |
| 11    | (–)          | ✓            | (–)          | ✓            | (–)       | ✓         | ✓            | (–)          | ✓         | (–)       | (–)        | ✓          | <b>Convergence</b>     |
| 12    | ✓            | (–)          | (–)          | ✓            | (–)       | ✓         | ✓            | (–)          | ✓         | (–)       | (–)        | ✓          | Convergence            |
| 13    | (–)          | ✓            | (–)          | ✓            | (–)       | ✓         | ✓            | (–)          | ✓         | (–)       | ✓          | ✓          | Convergence            |
| 14    | ✓            | (–)          | (–)          | ✓            | (–)       | ✓         | (–)          | ✓            | (–)       | ✓         | ✓          | ✓          | Convergence            |
| 15    | ✗            | (–)          | (–)          | ✓            | (–)       | ✓         | (–)          | ✓            | (–)       | ✓         | (–)        | ✓          | Severe Non-Convergence |
| 16    | (–)          | ✓            | ✓            | (–)          | ✓         | (–)       | ✓            | (–)          | ✓         | (–)       | (–)        | ✓          | Severe Non-Convergence |
| 17    | (–)          | ✓            | ✓            | (–)          | ✓         | (–)       | ✓            | (–)          | ✓         | (–)       | ✓          | ✓          | Convergence            |

Trials 1–2 considered most or all twelve parameters to explore the minimization, but failed, indicating too many parameter variations are unsuitable; the opposite approach (starting from fewer unconstrained parameters) bore fruit. Once all trials were completed, the final solution set was determined by computing *RPE* and performing comparisons in each converging trial pair, and selecting the parameter set that converged via the smallest total parameter (norm) perturbation. This filtering strategy (minimum norm transition heuristic) was conducted since larger parameter differences also induce more drastic departures from the original model parameters published in [41]. The termination tolerance for parameter estimation in our MATLAB optimization code was  $1 \cdot 10^{-8}$ , and the final parameter values were obtained by refining the termination criteria to the said value only after *RPE* yields the best trial (refinement requires 20% longer CPU time; Trial 11: 5.27 min vs. 4.37 min). The *RPE* values achieved vs. the respective warm fermentation simulations for the same  $T(t)$  profile and the parameter values for the Trial 11 set, for each of the three  $T(t)$  profiles, are shown in Table 8.

**Table 8.** *RPE* for Trial 11 and corresponding parameter values for the three  $T(t)$  profiles (bold: final).

| Symbol        | CCF<br>( $T = 5^\circ\text{C}$ ) | <i>RPE</i><br>( $T = 5^\circ\text{C}$ ) | CCF<br>( $T = 6.5^\circ\text{C}$ ) | <i>RPE</i><br>( $T = 6.5^\circ\text{C}$ ) | CCF<br>( $T = 5-6.5^\circ\text{C}$ )   | <i>RPE</i><br>( $T = 5-6.5^\circ\text{C}$ ) |
|---------------|----------------------------------|---|------------------------------------|---|--|---|
| $\mu_{AB}$    | (–)                              | (–)                                     | (–)                                | (–)                                       | (–)                                    | (–)   |
| $\mu_{DY}$    | $7.80 \cdot 10^{-6}$             | –93.890                                 | $7.27 \cdot 10^{-6}$               | –94.308                                   | <b><math>7.59 \cdot 10^{-6}</math></b> | <b>–94.054</b>                              |
| $B_{YEA}$     | (–)                              | (–)                                     | (–)                                | (–)                                       | (–)                                    | (–)   |
| $A_{YEA}$     | 123.040                          | 36.832                                  | 136.724                            | 52.051                                    | <b>169.130</b>                         | <b>88.090</b>                               |
| $B_{\mu e0}$  | (–)                              | (–)                                     | (–)                                | (–)                                       | (–)                                    | (–)   |
| $A_{\mu e0}$  | 2.903                            | –11.206                                 | 4.733                              | 44.744                                    | <b>4.125</b>                           | <b>26.148</b>                               |
| $A_{kes}$     | (–)                              | (–)                                     | (–)                                | (–)                                       | (–)                                    | (–)   |
| $B_{kes}$     | 34,658.614                       | 1.329                                   | 35,474.587                         | 3.714                                     | <b>35,203.709</b>                      | <b>2.922</b>                                |
| $A_{\mu X0}$  | 84.280                           | –22.185                                 | 69.395                             | –35.929                                   | <b>37.450</b>                          | <b>–65.423</b>                              |
| $B_{\mu X0}$  | (–)                              | (–)                                     | (–)                                | (–)                                       | (–)                                    | (–)   |
| $A_{\mu S0}$  | (–)                              | (–)                                     | (–)                                | (–)                                       | (–)                                    | (–)   |
| $B_{\mu S0}$  | 11,370.511                       | –2.437                                  | 11,950.314                         | 2.536                                     | <b>11,754.776</b>                      | <b>0.859</b>                                |
| $A_{\mu SD0}$ | (–)                              | (–)                                     | (–)                                | (–)                                       | (–)                                    | (–)   |
| $B_{\mu SD0}$ | (–)                              | (–)                                     | (–)                                | (–)                                       | (–)                                    | (–)   |
| $A_{\mu DT}$  | (–)                              | (–)                                     | (–)                                | (–)                                       | (–)                                    | (–)   |
| $B_{\mu DT}$  | (–)                              | (–)                                     | (–)                                | (–)                                       | (–)                                    | (–)   |
| $A_{\mu L}$   | (–)                              | (–)                                     | (–)                                | (–)                                       | (–)                                    | (–)   |
| $B_{\mu L}$   | (–)                              | (–)                                     | (–)                                | (–)                                       | (–)                                    | (–)   |

Table 8 shows a clear (but acceptable) parameter dependence on each  $T(t)$  profiles postulated (this is an artifact, as Table 5 offers only a few initial and final points for constraining the estimation). The response curves resulting from the implementation of the new (bold) parameters in Table 8 are plotted to confirm that the newly parameterized CCF model system replicates the industrial results, using the linearly increasing temperature profile,  $T = 5\text{--}6.5$  °C over the batch duration of  $t_{\text{span}} = 60$  h. Figure 9 presents the dynamic state responses for this nonisothermal  $T(t)$  profile, which is plausible due to exothermic fermentation reactions; the biomass activation is gradual and much slower vs. Figure 4.

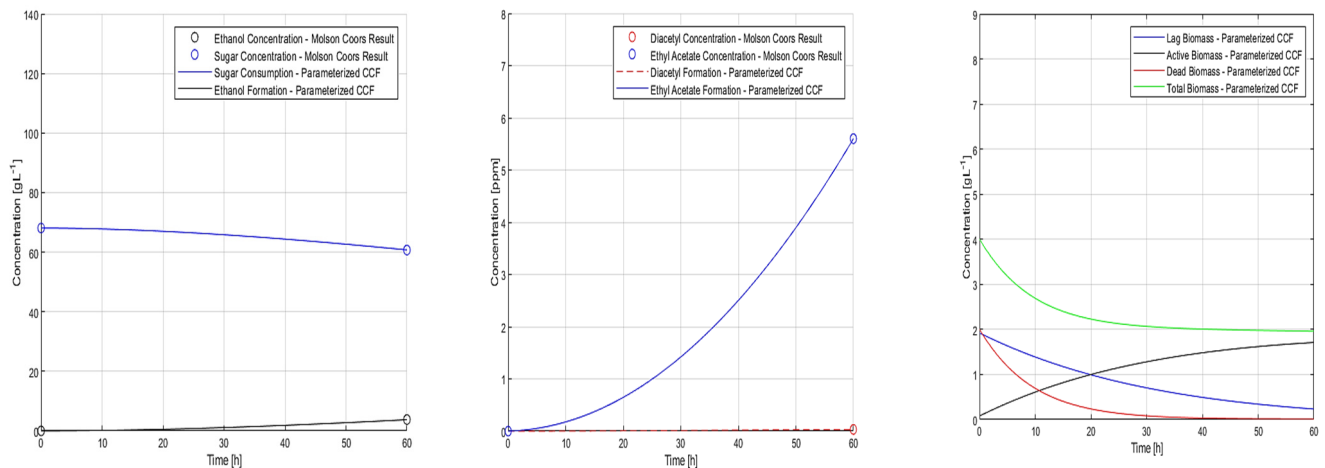


**Figure 9.** Reparameterized model results: sugar, ethanol, biomass, diacetyl, and ethyl acetate responses (Trial 11).

Sugar, ethanol, ethyl acetate, and diacetyl responses were plotted to analyze CCF (Figure 9). Reparameterized model responses of sugar and ethanol concentration match both the initial and final industrial data points. The smooth shape of both curves features a slow decrease rate for sugar consumption and a slow increase rate for ethanol formation, over the entire course of fermentation. Biomass fraction responses are also plotted (Figure 9); because industrial biomass data are not provided, the respective biomass curves are unconstrained functions in our foregoing reparameterization. Diacetyl concentrations are about two orders of magnitude smaller than warm fermentation values, while diacetyl dynamics are simpler (monotonic) due to very slow evolution, in contrast to Figure 4. Ethyl acetate concentration, though, is clearly higher (by about an order of magnitude) compared with the final-time warm fermentation values, as already evident by comparing Figure 4 vs. Table 5 values.

Table 9 summarizes the full parameter set for the reparameterized CCF model (including those that were chosen to remain unchanged), as well as diacetyl formation and consumption rates. Boldface denotes new CCF parameter values; the rest remain as per de Andrés-Toro et al. model [41]. The new CCF parameter values only best correspond to the specific  $T(t)$  profile and shift for others, as evident in Table 8 (any slight profile variation, even for either isothermal, yields different values). This is not only due to the given uncertainty in the industrial run from which Table 5 data emerged, but also due to the limited (loose) constraining of the CCF model, and the lack of mid-point  $C(t)$  data.

**Table 9.** Warm fermentation parameters of de Andrés-Toro et al. [41] and new CCF values (bold: this study).

| Rates and Factors | Description                                     | $A_i$          | $B_i$                          |
|-------------------|---|----------------|--------------------------------|
| $\mu_{SD0}$       | Maximum dead cell settling rate                 | 33.820         | −10,033.280                    |
| $\mu_{x0}$        | Maximum cell growth rate                        | <b>37.450</b>  | −31,934.090                    |
| $\mu_{S0}$        | Maximum sugar consumption rate                  | −41.920        | <b>11,754.776</b>              |
| $\mu_{e0}$        | Maximum ethanol production rate                 | <b>4.125</b>   | −1267.240                      |
| $\mu_{DT}$        | Specific cell death rate                        | 130.160        | −38,313.000                    |
| $\mu_L$           | Specific cell activation rate                   | 30.720         | −9501.540                      |
| $k_e = k_S$       | Affinity constant for sugar and ethanol         | −119.630       | <b>35,203.709</b>              |
| $Y_{EA}$          | Stoichiometric factor, ethyl acetate production | <b>169.130</b> | −26,589.000                    |
| $\mu_{DY}$        | Rate of diacetyl production                     |                | <b>7.590</b> ·10 <sup>−6</sup> |
| $\mu_{AB}$        | Rate of diacetyl consumption                    |                | 1.138·10 <sup>−3</sup>         |

### 5.3. Summary

The MATLAB parameter estimation code we developed employs the Nelder–Mead direct search algorithm to reparameterize the de Andrés-Toro et al. model [41] to describe CCF process conditions. Performance strongly depends on initial guess vector ( $x_0$ ) and understanding of change directions for each parameter, to successively add/remove  $x_0$  components and arrive at a converged solution set  $x_f$ . The standard least-squares regression objective was used for all CCF parameterization trials, and the various converged solutions ( $x_f$ ) were filtered via *RPE* to obtain the best parameter vector, i.e., that with the shortest deviation vs. the warm fermentation case, for the most realistic CCF  $T(t)$  profile. The complete CCF parameterized model is thus provided by Equations (5)–(23), with data from Tables 8 and 9.

## 6. Sensitivity Analysis

Sensitivity analyses are performed on dynamic models for a given set of operating conditions, with respect to changes in target model parameters. They provide further understanding of dynamic system responses and are essential prior to optimization [24]. This extra level of model understanding is critical for batch and semi-batch operations that can exhibit very low sensitivity to control policies. Sensitivity  $S$  quantifies state variable variation with respect to model parameter changes [47–50], as:

$$S = \left[ \left( \frac{\partial \theta}{\theta} \right) / \left( \frac{\partial P}{P} \right) \right] \quad (29)$$

where  $\theta$  denotes the vector of dynamic states of interest,  $P$  is the parameter vector that varies, and  $\partial \theta$ ,  $\partial P$  are the corresponding state and parameter changes (finite differences), respectively. Large sensitivities provide insight, implying parameters whose uncertain (inaccurate) estimation can induce enormous model vs. process output deviations, hence must be carefully assessed for control. Low sensitivities, accordingly, imply that parameter estimation errors have limited operational effect.

Sensitivity analyses are local or global: the former consider small parameter perturbations, while the latter explore effects of large and/or simultaneous parameter changes on model fidelity [48–50]. We focus here on local sensitivity analyses performed for  $\pm 5\%$  and  $\pm 25\%$  parameter variation for each of the set of 12 potentially crucial parameters (variation above 25% induces severe non-convergence issues within DAE). Variations in 5% are sufficiently small to show sensitivity differences between different model parameters, maintaining relevance to our *RPE* values from parameterization trials.

Final key compound concentration sensitivities are computed and are illustrated in Figures 10–12.

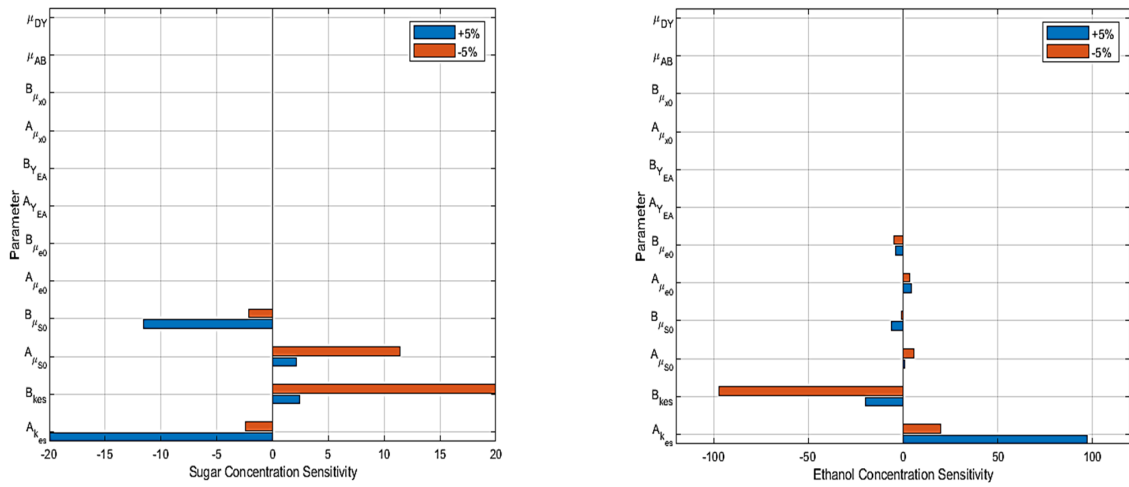


Figure 10. Sugar (left) and ethanol (right) concentration response sensitivity for a  $\pm 5\%$  change in 12 parameters.

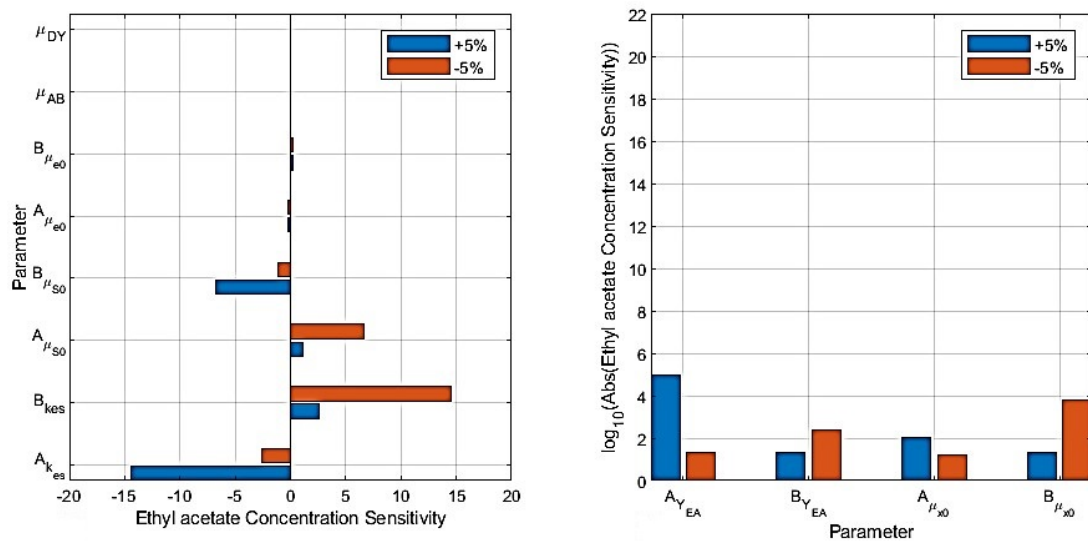


Figure 11. Ethyl acetate concentration response sensitivity for a  $\pm 5\%$  change in the 12 parameters.

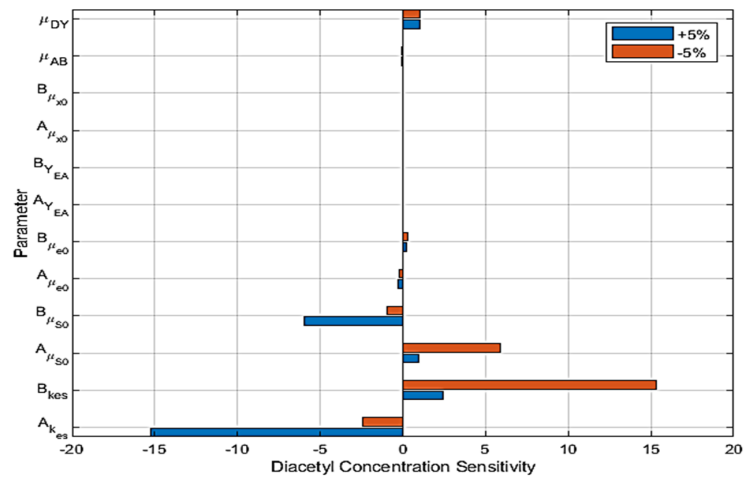


Figure 12. Diacetyl concentration response sensitivity for a  $\pm 5\%$  change in the 12 parameters.

Sugar concentration ( $C_S$ ) is most sensitive to changes in the parameters  $A_{kes}$  and  $B_{kes}$ , followed by the effects of variations in  $A_{\mu S0}$  and  $B_{\mu S0}$ . Though the effect of parameter variation on final sugar concentration appears to be inverted for parameter pairs, this is not always the case, as shown in succeeding sensitivity analyses. Actual values for all remaining pairs are on the order of  $1 \cdot 10^{-9}$ – $1 \cdot 10^{-8}$  (very close to solver tolerance,  $1 \cdot 10^{-9}$ ), rendering final sugar concentration sensitivity insignificant.

Final ethanol concentration ( $C_E$ ) sensitivity to  $\pm 5\%$  parameter changes is illustrated in Figure 10. Here, as for  $C_S$ ,  $A_{kes}$  and  $B_{kes}$  variations again produce the largest final ethanol concentration changes. The sensitivity of final ethanol concentration is roughly five times larger (for  $A_{kes}$  and  $B_{kes}$  variation) than the sensitivity of final sugar concentration to identical  $A_{kes}$  and  $B_{kes}$  changes, but of opposite sign. Variations in  $A_{\mu S0}$ ,  $B_{\mu S0}$ ,  $A_{\mu e0}$ , and  $B_{\mu e0}$  produce similarly sized changes in final ethanol concentration. All other sensitivity values for other target parameters are in the order of  $1 \cdot 10^{-8}$ , hence insignificant.

Final ethyl acetate concentration ( $C_{EA}$ ) sensitivity to  $\pm 5\%$  parameter changes is shown in Figure 11: therein,  $A_{YEA}$  and  $B_{\mu x0}$  emerge as most influential on ethyl acetate concentration, followed by  $B_{YEA}$  and then  $A_{\mu x0}$  and all remaining parameters depicted. Sensitivity values for  $\mu_{AB}$  and  $\mu_{DY}$  are on the order of  $1 \cdot 10^{-8}$ – $1 \cdot 10^{-7}$ , and for the foregoing reasons, insignificant vs. final ethyl acetate ( $C_{EA}$ ) concentrations.

Final diacetyl concentration ( $C_{DY}$ ) sensitivity to  $\pm 5\%$  parameter changes is presented in Figure 12:  $A_{kes}$  and  $B_{kes}$  have the strongest impact, followed by  $A_{\mu S0}$ ,  $B_{\mu S0}$ , and  $\mu_{DY}$ . The two parameters directly related to diacetyl formation and consumption ( $\mu_{DY}$  and  $\mu_{AB}$ ) do not induce the largest sensitivity (other parameter sensitivities are of the order of  $10^{-6}$ , their effect hence being insignificant).

Final ethyl acetate concentration is by far the most sensitive to parameter variation, followed by ethanol, sugar, and diacetyl responses;  $C_{EA}$  sensitivity is highest for  $A_{YEA}$  changes, while all other state variables respond strongest to  $A_{kes}$  and  $B_{kes}$  variations. Clearly, small CCF initial condition and/or  $T(t)$  changes may induce key model response drifts, implying critical process (product quality) variation. The high sensitivity of many responses to  $A_{kes}$  and  $B_{kes}$  changes is justified by recognizing that they directly affect sugar consumption and ethanol formation, and indirectly (through ethanol) diacetyl levels. Sugar concentration is critical [51]: it governs biomass proliferation which drives ethanol, diacetyl, and esters formation. Thus, all parameters affecting  $C_S$  and  $C_E$  induce composite (synergistic) effects. Conversely,  $A_{\mu x0}$  and  $B_{\mu x0}$  variation generally induce minimal response change (excluding  $C_{EA}$  levels).

## 7. Coarse Grid Enumeration of Plausible Temperature Manipulation Profiles

A conceptual CCF process may operate in a tight ( $1.5^\circ\text{C}$ ) temperature band ( $T = 5$ – $6.5^\circ\text{C}$ ), although it is recognized that CCF can be performed for  $T = 0$ – $8^\circ\text{C}$  [8,14,16–20]. The use of cooling jackets allows for implementing industrial fermentation  $T(t)$  profiles with temperature changes, provided that the fermentor is not cooled excessively and that enough reaction heat is produced [20]. Our goal is to gain insight into responses computed from our CCF model parameterization for different plausible  $T(t)$  profiles, beyond isothermal or tightly restricted ‘constant and increasing’ ones.

Quantifying the effects of imposed  $T(t)$  profile variability on final-time beer quality is achieved via monitoring the respective vector of concentrations,  $[C_S(t = t_f), C_E(t = t_f), C_{EA}(t = t_f), C_{DY}(t = t_f)]^T$ . Multiobjective process optimization for brewing intensification at lower cost with flavor consistency has been the focus of many studies on warm (but few on cold) fermentation over three decades [20–24,30–44]. To comprehensively explore operational options in a wide temperature range, we can construct a set of feasible  $T(t)$  manipulation profiles and evaluate the resulting final-time concentration vectors [20].

To enumerate plausible  $T(t)$  manipulation profiles, the CCF time domain (60 h) is discretized into an initial ‘coarse grid’ (6 intervals; 10 h each). The temperature domain is discretized in six  $1^\circ\text{C}$  intervals, from  $T = 1^\circ\text{C}$  up to and including  $T = 7^\circ\text{C}$ , yielding a 36-block canvas of 49 nodes (Figure 13). This larger, more inclusive  $T(t)$  span is selected

based on the theoretical range (0–8 °C) reported in the literature [8,14,16–20], and is constrained because operating at  $T < 1$  °C outside of a laboratory is unrealistic (too close to water freezing is very problematic for industrial operations and instruments). Temperatures  $T > 7$  °C are omitted for the reasons underlying the de Andrés-Toro et al. model [41]. Finer time grids are possible (at extra CPU expense), but finer  $T(t)$  grids are pointless vs. sensing.

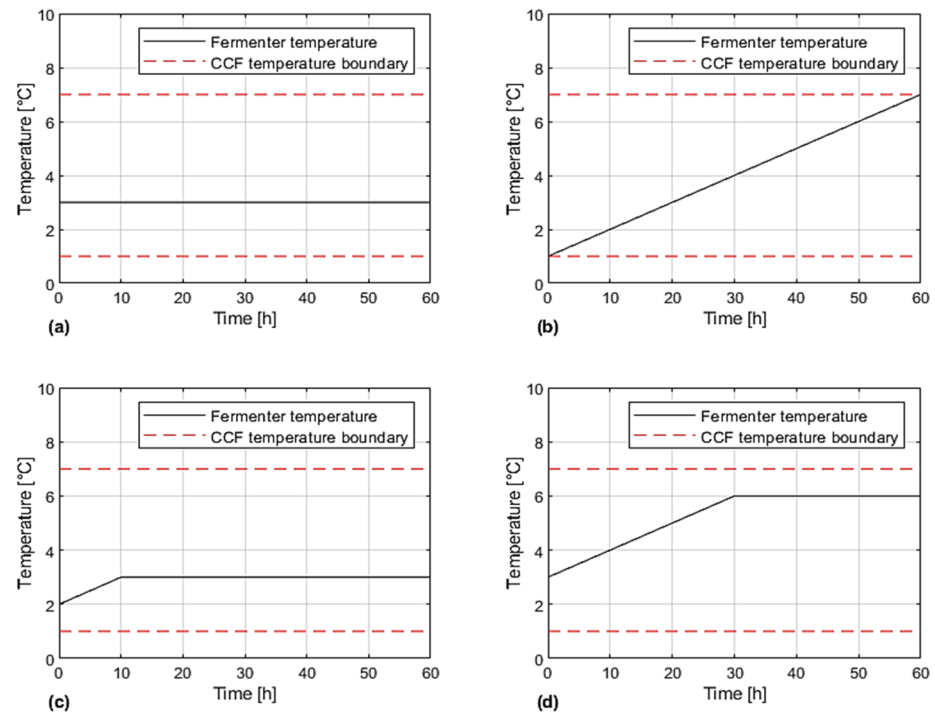


**Figure 13.** Four temperature profile types: (a) isothermal, (b) increasing without any constant segments, (c) increasing for one time step, then constant, (d) increasing for multiple time steps, then constant.

### 7.1. Heuristics for Plausible Temperature Manipulation Profiles

To perform enumeration, we use a set of heuristics to limit the ensemble of plausible  $T(t)$  profiles. The rationalizations for many of them emerge conceptually from published cost functions for beer fermentation control optimization via deterministic or stochastic (genetic) algorithms [20–22,41–43]. This happens for two reasons: to ensure  $T(t)$  profiles correspond to feasible industrial manipulations, but also to achieve a tractable total number of plausible  $T(t)$  profiles within reasonable CPU expense.

Heuristic 1: Temperature profiles can be isothermal along the entire computational domain.

Reasoning: Fermentations may progress with  $T$  changes smaller than detectable instrum. limits (1 °C).

Heuristic 2: Temperature profiles can monotonically increase in the entire fermentation time domain.

Reasoning: Fermentations may result in increasing batch temperatures throughout the CCF process.

Heuristic 3: The CCF process may begin and end at any temperature between  $T = 1$  and 7 °C.

Reasoning: The said temperature range for CCF operation is established in the literature [1–3,9].

Heuristic 4: The temperature difference between successive time nodes may not exceed 1 °C.

Reasoning: Implemented to reflect operability vs. curse of dimensionality (fewer plausible  $T$  profiles).

Heuristic 5: Any number of isothermal segments (10 h) can succeed any number of increasing T ones.

Reasoning: Fermentations may progress as a mix of isothermal and exothermic segments in the vessel.

Heuristic 6: A time period of increasing temperature cannot succeed a period of isothermal activity.

Reasoning: The fermentation process is continuous and assumed here to exclude effects of hysteresis.

Heuristic 7: The temperature in the fermenter cannot decrease at any point.

Reasoning: Excessive CCF cooling obstructs biochemical activity, effectively delaying fermentation.

### 7.2. Effect of Total Theoretical Heat Input on Final-Time CCF Concentrations

The said heuristics enable the classification of plausible  $T(t)$  manipulation profiles in four groups (Figure 13): temperature profiles used, corresponding trial numbers, and types, are detailed in Table 10. Trials are classified by total theoretical heat input ( $Q$ ), from lowest (Trial 1) to highest (Trial 29) value.

**Table 10.** Candidate CCF temperature manipulation profiles ( $^{\circ}\text{C}$ ) ranked vs.  $Q$  (Trial 23: threshold).

| $T(t)$ Trial | $T(t = 0)$ | $T(t = 10)$ | $T(t = 20)$ | $T(t = 30)$ | $T(t = 40)$ | $T(t = 50)$ | $T(t = 60)$ | Type |
|--------------|------------|-------------|-------------|-------------|-------------|-------------|-------------|------|
| 1            | 1          | 1           | 1           | 1           | 1           | 1           | 1           | a    |
| 2            | 1          | 2           | 2           | 2           | 2           | 2           | 2           | c    |
| 3            | 2          | 2           | 2           | 2           | 2           | 2           | 2           | a    |
| 4            | 1          | 2           | 3           | 3           | 3           | 3           | 3           | d    |
| 5            | 2          | 3           | 3           | 3           | 3           | 3           | 3           | c    |
| 6            | 3          | 3           | 3           | 3           | 3           | 3           | 3           | a    |
| 7            | 1          | 2           | 3           | 4           | 4           | 4           | 4           | d    |
| 8            | 1          | 2           | 3           | 4           | 5           | 5           | 5           | d    |
| 9            | 2          | 3           | 4           | 4           | 4           | 4           | 4           | d    |
| 10           | 3          | 4           | 4           | 4           | 4           | 4           | 4           | c    |
| 11           | 1          | 2           | 3           | 4           | 5           | 6           | 6           | d    |
| 12           | 4          | 4           | 4           | 4           | 4           | 4           | 4           | a    |
| 13           | 1          | 2           | 3           | 4           | 5           | 6           | 7           | b    |
| 14           | 2          | 3           | 4           | 5           | 5           | 5           | 5           | d    |
| 15           | 2          | 3           | 4           | 5           | 6           | 6           | 6           | d    |
| 16           | 3          | 4           | 5           | 5           | 5           | 5           | 5           | d    |
| 17           | 4          | 5           | 5           | 5           | 5           | 5           | 5           | c    |
| 18           | 2          | 3           | 4           | 5           | 6           | 7           | 7           | d    |
| 19           | 5          | 5           | 5           | 5           | 5           | 5           | 5           | a    |
| 20           | 3          | 4           | 5           | 6           | 6           | 6           | 6           | d    |
| 21           | 3          | 4           | 5           | 6           | 7           | 7           | 7           | d    |
| 22           | 4          | 5           | 6           | 6           | 6           | 6           | 6           | d    |
| 23           | 5          | 5.25        | 5.5         | 5.75        | 6           | 6.25        | 6.5         | (-)  |
| 24           | 5          | 6           | 6           | 6           | 6           | 6           | 6           | c    |
| 25           | 6          | 6           | 6           | 6           | 6           | 6           | 6           | a    |
| 26           | 4          | 5           | 6           | 7           | 7           | 7           | 7           | d    |
| 27           | 5          | 6           | 7           | 7           | 7           | 7           | 7           | d    |
| 28           | 6          | 7           | 7           | 7           | 7           | 7           | 7           | c    |
| 29           | 7          | 7           | 7           | 7           | 7           | 7           | 7           | a    |

The total theoretical heat input ( $Q$ ) provided to the CCF fermentor mixture (ignoring losses) is:

$$Q = mC_p \int_{t_0}^{t_f} T(t) dt \quad (30)$$

where  $Q$  is the theoretical heat input,  $m$  is the fermentation mass,  $C_p$  is the specific heat capacity of the mixture,  $T(t)$  is the fermentor temperature and time  $dt$  spans the fermentation interval  $t = 0\text{--}60$  h. This definition is operationally equivalent to the total theoretical enthalpy of the mixture at any time, as  $T(t)$  is the net effect of exothermic CCF reactions and heat removal from the system (cooling jacket). Actual industrial fermentor heat transfer dynamics are a lot more complex, but easy to address [23]. Specific  $Q$  values are not provided, as they are only used for ranking and plotting final concentrations (Figure 14).

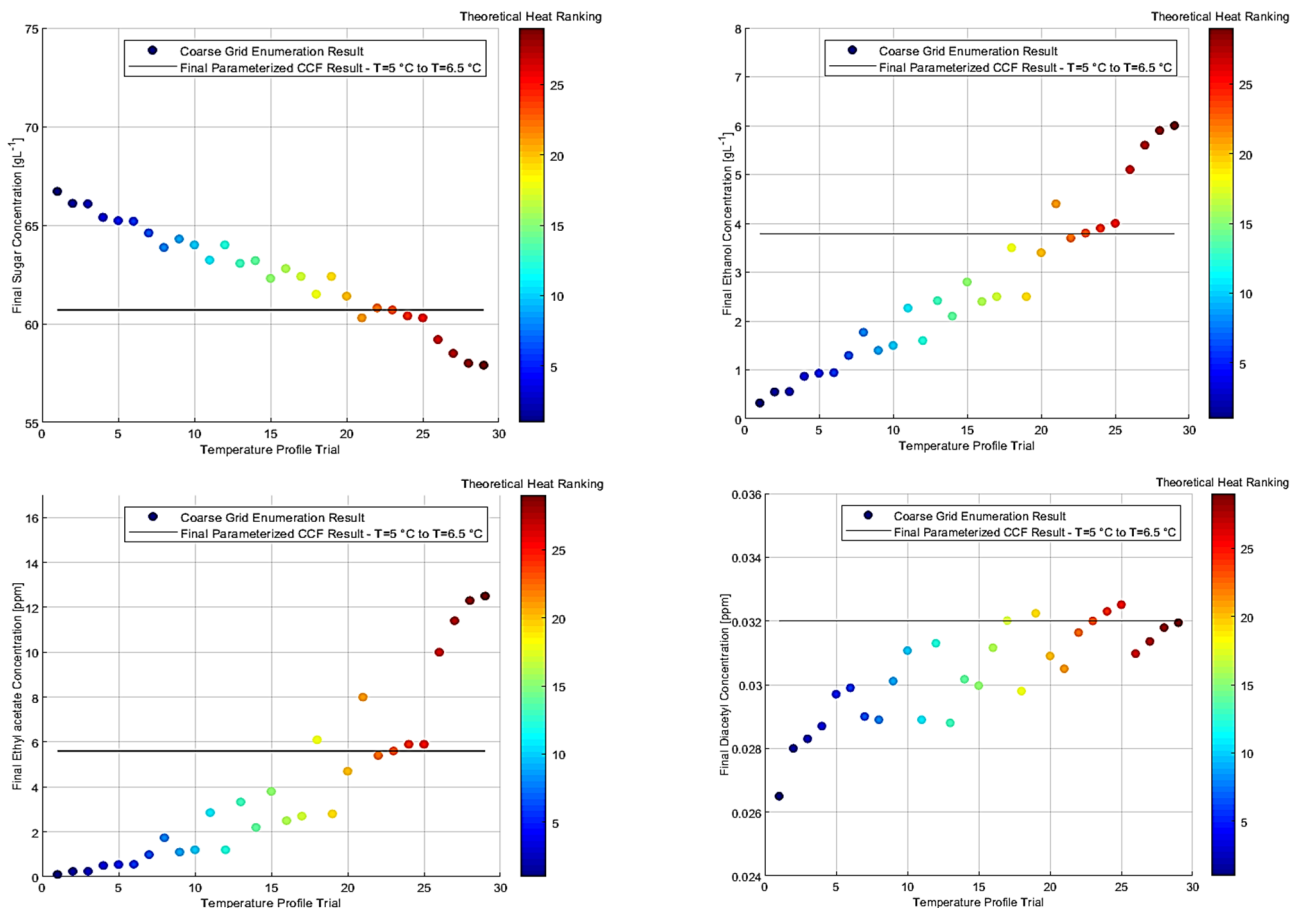


**Figure 14.** Final sugar (top left), ethanol (top right), ethyl acetate (bottom left), and diacetyl (bottom right) concentration from profile enumeration, vs. respective base-case values from CCF model (black lines).

Final sugar concentration ( $C_S$ ) ranges between 57.9 and 66.7  $\text{g}\cdot\text{L}^{-1}$  for the  $T(t)$  profiles of Table 10, implying higher heat input ( $Q$ ) induces greater sugar consumption up to Trial 8 and after Trial 21; the respective segments (Trials 1–8, 21–26) appear monotonic, whereas Trials 9–20 show oscillations.

Final ethanol concentration ( $C_E$ ) ranges between 0.3 and 6.0  $\text{g}\cdot\text{L}^{-1}$  for the same temperature profiles, (a 20-fold span depending on  $T(t)$  variation), also increasing as a function of theoretical heat input  $Q$ . Trials 8–26 again show oscillation in between linear trends; this is key for CCF ethanol minimization.

Another important conclusion is drawn by observing the right end of all four panels of Figure 14. Response grouping for Trials 22–25 and 26–29, indicate two sets of CCF processes which are very similar in terms of total theoretical heat input (thus resulting in very similar expression of ethanol), but also very different in terms of flavor compound (diacetyls, esters) expressions in the final product. A distinct jump is remarkable between Trials 25 and 26; in the latter, a high  $T = 7^\circ\text{C}$  is used for 40 h. This clearly implies a hard

thermal threshold which must be avoided during industrial CCF runs, given the definitive requirement for low final ethanol (perhaps also low total ester) concentrations.

Final ethyl acetate concentration ( $C_{EA}$ ) ranges between 0.1 and 12.5 ppm for the temperature profiles, and it is generally (not always, e.g., Trials 8–19) increasing as a function of theoretical heat input ( $Q$ ). Trials 1–8 have a linear trend, before the oscillatory behavior. A 70% jump between Trials 25 and 26 (using  $T = 7$  °C for 40 h or longer), implies a threshold to be avoided, to prevent a high- $Q$   $C_{EA}$  surge. Figure 14 shows a potentially useful high  $C_{EA}$  sensitivity to small temperature changes: a small heat input change can strongly impact ester expression (Trials 25–26) without comparable changes in other flavor compounds, esp. as esters are typically near or just above beer flavor threshold values [20–24]. Minor process changes can induce beneficial flavor variations, as esters boost fruitiness (cf. Table 6).

Final diacetyl concentration ( $C_{DY}$ ) ranges between 2.6 and  $3.2 \cdot 10^{-2}$  ppm for these temperature profiles and remains in all cases (Trials 1–29) within specifications (26–32 ppb) (cf. different  $C_{EA}$  vs.  $C_{DY}$  scales). Final  $C_{DY}$  generally rises with  $T(t)$  profiles of higher  $Q$ , with pronounced oscillations after Trial 6. Flavor thresholds for  $C_{EA}$  and  $C_{DY}$  are of the same order of magnitude, so our reparameterized model implies there is great potential for beneficial ester (vs. diacetyl) expression under CCF conditions [33].

A set of four different temperature profile types (based on seven constraint heuristics) were used for CCF model response enumeration, in the acceptable temperature range of 1–7 °C. Employing a coarse time grid discretization, dynamic simulations were ranked by total theoretical heat input ( $Q$ ) received by the fermentation system, yielding a series of colormaps illustrating temperature profile variation effects on key final observable (sugar, ethanol, diacetyl, and ethyl acetate) concentrations.

Simulations for higher theoretical heat ( $Q$ ) show higher sugar consumption and higher ethanol, ethyl acetate, and diacetyl production for warm brewing [20–24]. Temperature profiles of  $T = 7$  °C for 40 h or more yield a surge in ethanol and ethyl acetate production, and high sugar consumption. Diacetyl expression varies much less (within 6 ppb), implying ethanol and ethyl acetate sensitivities are of much greater concern. Identical theoretical heat ( $Q$ ) inputs may have very different effects, depending on the CCF  $T(t)$  profile chosen. Though a concern from a process control perspective, this may enable small but extremely beneficial to flavor changes without any major process modifications.

## 8. Conclusions

CCF is one of the best LAB/AFB brewing methods due to simplicity, cost-effectiveness, and limited alterations required to fermentation step temperature profile and duration. Modern industrial implementation attests to its efficiency vs. other methods developed over the last few decades [3,9]. Concerns regarding flavor remain: this paper aims to not only explore  $T(t)$  effects and response outputs between warm fermentation and CCF, but also to construct a reparameterized model which accurately describes the physical CCF process with regard to hypothetical changes and sensitivities.

The de Andrés-Toro et al. first-principles model [41] was used due to its predictive fidelity and the concise number of data points available for validation. The MATLAB (DAE) code constructed matches and published model simulations for  $T = 13$  °C, and was used for quantitative comparisons between warm fermentation and CCF model responses. A CCF model reparameterization via industrial data (initial and final sugar, ethanol, diacetyl, and ethyl acetate values) and sensitivity analysis followed. Finally, a ‘coarse grid enumeration’ was performed to analyze the effect of plausible  $T(t)$  profiles on CCF brewing, showing reduced ethanol production generally coincides with lower flavor expression.

Model reparameterization is instrumental, as per *RPE* comparisons between model responses for CCF vs. de Andrés-Toro et al. ( $T = 13$  °C) process conditions: CPU expense is relatively small but varies widely with trial conditions. Convergence and speed depend on parameter subset selection. The Nelder–Mead algorithm with least-squares regression performed well in this study, yielding parameter values which achieved full CCF model

matching against the concise industrial dataset used. New CCF parameters are not vastly departed from warm brewing [20–24,41], with  $RPE$  within an order of magnitude; future efforts must use larger datasets and global optimization algorithms [49].

A sensitivity analysis indicates that parameters  $A_{kes}$  and  $B_{kes}$  are the strongest influencers of response variation, due to the great importance of sugar, ethanol, and biomass in model dynamics. Ethyl acetate is the most sensitive response vs. parameter variations, confirming that ester expression is an indispensable LAB/AFB process control target, given its dominance on fruitiness perception.

Coarse grid enumeration reveals a global increase trend for sugar consumption and ethanol, ethyl acetate, and diacetyl formation with increasing theoretical heat input ( $Q$ ). Ethanol and especially ethyl acetate formation are most sensitive to  $T(t)$  profile variation, with output variation ranges much larger than sugar consumption and diacetyl formation. Results clustering show that small  $T(t)$  profile changes can greatly benefit product flavor and quality. A trade-off is clear, as CCF aims for ethanol reduction without flavor loss, but targets all rise together, yet at different rates. Experiments for flavor improvement may result in higher ethanol expression, but post-process dilution compromises flavor. Product refinement must focus on relative flavor compound change rates within narrow temperature intervals, possibly smaller batches, and external preheating/cooling/agitation for best process control.

The development of select  $T(t)$  profiles indicates that not all are necessarily possible without heat exchange (cooling) during CCF. For any given hypothetical  $T(t)$  profile with a confirmed promise of improved results over current CCF, extra capital expenditure is needed that may offset AFB profits, as fermenters typically comprise only cooling jackets. When the resulting AFB product is of superior flavor and quality (confirmed via simulations and pilot plant experiments), the benefit is warranted.

Multiobjective CCF optimization requires much larger datasets (more measured inputs/outputs, higher data density), as biomass responses here (and CCF mid-time points) are left unconstrained. Performing ‘what if’ analyses (e.g., enumeration) requires more extensive CCF model validation to accurately predict  $T(t)$  profile variation effects within tight ranges. No consideration of yeast strain effects, initial sugar/biomass concentration, and fermentation duration is considered here (all are assumed constant due to industrial conditions). The best process in terms of flavor, quality, and processing time can emerge from a combined approach, using additional processing steps and/or treatment methods (pre-/post-processing), after evaluating the impact of manipulations on efficiency.

Though the de Andrés-Toro et al. model is powerful via its reduced number of state variables, additional flavor compounds must be considered to better capture more beer flavor dimensions. Dynamic models cannot easily capture bitterness or wortiness (due to carbonyls of e.g., acetaldehyde and 2-/3-methylbutanal), both compromising LAB/AFB flavor; however, more model compounds increase DOF and require larger datasets to ensure and maintain high model fidelity. Potential new parameterizations towards CCF intensification thus require data acquired over a finer time domain discretization, with more flavor coordinates and fewer temperature profile heuristics.

**Author Contributions:** Conceptualization, D.W.P. and D.I.G.; methodology, D.W.P. and D.I.G.; software, D.W.P.; validation, D.W.P.; formal analysis, D.W.P. and D.I.G.; writing, D.W.P. and D.I.G.; supervision, D.I.G.; project administration, D.I.G. All authors have read and agreed to the published version of the manuscript.

**Funding:** D.I.G. gratefully acknowledges financial support from the Engineering and Physical Sciences Research Council (EPSRC) and UKRI, under the auspices of an ongoing grant (RAPID—ReAl-time Process Modelling and Diagnostics—Powering Digital Factories, Grant No. EP/V028618/1).

**Institutional Review Board Statement:** Not applicable.

**Informed Consent Statement:** Not applicable.

**Data Availability Statement:** All data used are reported here and/or in the cited literature sources.

**Acknowledgments:** D.I.G. also gratefully acknowledges an earlier Royal Academy of Engineering (RAEng) Industrial Fellowship (2017–2018). Both authors gratefully acknowledge technical discussions with Molson Coors colleagues, as well as the financial support of the Engineering and Physical Sciences Research Council (EPSRC) via prior funding from an Impact Acceleration Account (IAA) as administered by Edinburgh Research and Innovation (ERI). Financial support by the Great Britain Sasakawa and Nagai Foundations helped us to present earlier versions of this study.

**Conflicts of Interest:** The authors declare no conflict of interest. The funders had no role in the study. Tabulated and cited literature data suffice for reproducing original results; no other data are required for reproducibility.

## References

1. Southby, E.R. *A Systematic Handbook of Practical Brewing*; Franklin Classics: Oxford, UK, 1885.
2. Boulton, C.; Quain, D. *Brewing Yeast and Fermentation*; Elsevier: Amsterdam, The Netherlands, 2001.
3. Liguori, L.; Russo, P.; Albanese, D.; Di Matteo, M. Production of low-alcohol beverages: Current status and perspectives. In *Food Processing for Increased Quality and Consumption*; Elsevier: Amsterdam, The Netherlands, 2018; pp. 347–382.
4. STATISTA. Beer Production Worldwide (1998–2018). Available online: [Statista.com/statistics/270275](https://www.statista.com/statistics/270275) (accessed on 1 May 2019).
5. Wunderlich, S.; Back, W. Overview of manufacturing beer: Ingredients, processes and quality criteria. In *Beer in Health & Disease Prevention*; Elsevier: Amsterdam, The Netherlands, 2009; pp. 3–16.
6. Pavsler, A.; Buiatti, S. Non-lager & Lager beer. In *Beer in Health & Disease Prevention*; Elsevier: Amsterdam, The Netherlands, 2009; pp. 17–43.
7. Shopska, V.; Denkova-Kostova, R.; Kostov, G. Modeling in brewing—A review. *Processes* **2022**, *10*, 267. [[CrossRef](#)]
8. Montanari, L.; Marconi, O.; Mayer, H.; Fantozzi, P. Production of alcohol-free beer. In *Beer in Health & Disease Prevention*; Elsevier: Amsterdam, The Netherlands, 2009; pp. 61–75.
9. Brányik, T.; Silva, D.P.; Baszczyński, M.; Lehnert, R.; e Silva, J.B.A. A review of methods of low alcohol and alcohol-free beer production. *J. Food Eng.* **2012**, *108*, 493–506. [[CrossRef](#)]
10. Liguori, L.; De Francesco, G.; Russo, P.; Perretti, G.; Albanese, D.; Di Matteo, M. Production and characterization of alcohol-free beer by membrane process. *Food Bioprod. Process.* **2015**, *94*, 158–168. [[CrossRef](#)]
11. Kyselová, L.; Brányik, T. Quality improvement and fermentation control in beer. In *Advances in Fermented Foods and Beverages*; Elsevier: Amsterdam, The Netherlands, 2015.
12. Blanco, C.A.; Caballero, I.; Barrios, R.; Rojas, A. Innovations in the brewing industry: Light beer. *Int. J. Food Sci. Nutr.* **2004**, *65*, 655–660. [[CrossRef](#)] [[PubMed](#)]
13. Catarino, M.D. Production of Non-Alcoholic Beer with Reincorporation of Original Compounds. Ph.D. Thesis, University of Porto, Porto, Portugal, 2010.
14. Sohrabvandi, S.; Mousavi, S.M.; Razavi, S.H.; Mortazavian, A.M.; Rezaei, K. Alcohol-free beer: Methods of production, sensorial defects, and healthful effects. *Food Rev. Int.* **2010**, *26*, 335–352. [[CrossRef](#)]
15. De Francesco, G.; Turchetti, B.; Sileoni, V.; Marconi, O.; Perretti, G. Screening of new strains of *Saccharomyces ludwigii* and *Zygosaccharomyces rouxii* to produce low-alcohol beer. *J. Inst. Brew.* **2015**, *121*, 113–121. [[CrossRef](#)]
16. Schur, F. Ein neues verfahren herstellung von alkoholfreien bier. In *Proceedings of the 19th European Brewery Convention Congress*; IRL Press: Oxford, UK, 1983; pp. 353–360.
17. Perpète, P.; Collin, S. Fate of the warty flavours in cold contact fermentation. *Food Chem.* **1999**, *66*, 359–363. [[CrossRef](#)]
18. Perpète, P.; Collin, S. How to improve the enzymatic warty flavour reduction in a cold contact fermentation. *Food Chem.* **2000**, *70*, 457–462. [[CrossRef](#)]
19. Mota, A.; Novák, P.; Macieira, F.; Vicente, A.A.; Teixeira, J.A.; Šmogrovičová, D.; Brányik, T. Formation of flavor-active compounds during continuous alcohol-free beer production. *J. Am. Soc. Brew. Chem.* **2010**, *69*, 1–7.
20. Rodman, A.D.; Gerogiorgis, D.I. Multi-objective process optimisation of beer fermentation via dynamic simulation. *Food Bioprod. Process.* **2016**, *100*, 255–274. [[CrossRef](#)]
21. Rodman, A.D.; Gerogiorgis, D.I. Dynamic optimization of beer fermentation: Sensitivity analysis of attainable performance vs. product flavour constraints. *Comput. Chem. Eng.* **2017**, *106*, 582–595. [[CrossRef](#)]
22. Rodman, A.D.; Fraga, E.S.; Gerogiorgis, D. On the application of a nature-inspired stochastic evolutionary algorithm to constrained multi-objective beer fermentation optimisation. *Comput. Chem. Eng.* **2018**, *108*, 448–459. [[CrossRef](#)]
23. Rodman, A.D.; Weaser, M.; Griffiths, L.; Gerogiorgis, D. I. Dynamic optimisation and visualisation of industrial beer fermentation with explicit heat transfer dynamics. *Comput. Aid. Chem. Eng.* **2019**, *46*, 1459–1464.
24. Rodman, A.D.; Gerogiorgis, D.I. Parameter estimation and sensitivity analysis for dynamic modelling and simulation of beer fermentation. *Comput. Chem. Eng.* **2020**, *136*, 106665. [[CrossRef](#)]
25. Parker, D.K. Beer: Production, sensory characteristics and sensory analysis. In *Alcoholic Beverages: Sensory Evaluation and Consumer Research*; Woodhead Publishing Limited: Thorston, UK, 2012.
26. Vanderhaegen, B.; Neven, H.; Verachtert, H.; Derdelinckx, G. The chemistry of beer aging—a critical review. *Food Chem.* **2006**, *95*, 357–381. [[CrossRef](#)]

27. Evellin, F.; Perpète, P.; Collin, S. Yeast ADHI disruption: A way to promote carbonyl compounds reduction in alcohol-free beer production. *J. Am. Soc. Brew. Chem.* **1999**, *57*, 109–113.
28. Purificación Hernández-Artiga, M.; Bellido-Milla, D. The evaluation of beer aging. In *Beer in Health & Disease Prevention*; Elsevier: Amsterdam, The Netherlands, 2009; pp. 913–922.
29. Baert, J.J.; De Clippeleer, J.; Hughes, P.S.; De Cooman, L.; Aerts, G. On the origin of free and bound staling aldehydes in beer. *J. Agric. Food Chem.* **2012**, *60*, 11449–11472. [[CrossRef](#)]
30. Strejc, J.; Siříšř'ová, L.; Karabín, M.; Almeida e Silva, J.B.; Brányik, T. Production of alcohol-free beer with elevated amounts of flavouring compounds using lager yeast mutants. *J. Inst. Brew.* **2013**, *119*, 149–155.
31. Gee, D.A.; Ramirez, W.F. A flavour model for beer fermentation. *J. Inst. Brew.* **1994**, *100*, 321–329. [[CrossRef](#)]
32. Perpète, P.; Collin, S. Contribution of 3-methylthiopropionaldehyde to the worty flavor of alcohol-free beers. *J. Agric. Food Chem.* **1999**, *47*, 2374–2378. [[CrossRef](#)]
33. Verstrepen, K.J.; Derdelinckx, G.; Dufour, J.P.; Winderickx, J.; Thevelein, J.M.; Pretorius, I.S.; Delvaux, F.R. Flavor-active esters: Adding fruitiness to beer. *J. Biosci. Bioeng.* **2003**, *96*, 110–188. [[CrossRef](#)]
34. Hellborg, L.; Piskur, J. Yeast diversity in the brewing industry. In *Beer in Health & Disease*; Elsevier: Amsterdam, The Netherlands, 2009; pp. 77–88.
35. Bokulich, N.A.; Bamforth, C.W. The microbiology of malting and brewing. *Microbiol. Mol. Biol. Rev.* **2013**, *77*, 157–172. [[CrossRef](#)] [[PubMed](#)]
36. Van Iersel, M.; Van Dieren, B.; Rombouts, F.; Abee, T. Flavor formation and cell physiology during the production of alcohol-free beer with immobilized *Saccharomyces cerevisiae*. *Enzyme Microb. Technol.* **1999**, *24*, 407–411. [[CrossRef](#)]
37. Van Iersel, M.F.M.; Brouwer-Post, E.; Rombouts, F.; Abee, T. Influence of yeast immobilization on fermentation and aldehyde reduction during the production of alcohol-free beer. *Enzyme Microb. Technol.* **2000**, *26*, 602–607. [[CrossRef](#)]
38. Engasser, J.M.; Marc, I.; Moll, M.; Duteurtre, B. Kinetic modeling of beer fermentation. *Congr. Eur. Brew. Conv.* **1981**, *18*, 579–586.
39. García, A.I.; García, L.A.; Díaz, M. Modeling of diacetyl production during beer fermentation. *J. Inst. Brew.* **1994**, *100*, 179–183. [[CrossRef](#)]
40. Pilarski, D.W.; Gerogiorgis, D.I. Progress and modelling of cold contact fermentation for alcohol-free beer production: A review. *J. Food. Eng.* **2020**, *273*, 109804. [[CrossRef](#)]
41. de Andrés-Toro, B.; Giron-Sierra, J.M.; Lopez-Orozco, J.A.; Fernandez-Conde, C.; Peinado, J. M.; García-Ochoa, F. A kinetic model for beer production under industrial operational conditions. *Math. Comput. Simul.* **1998**, *48*, 65–74. [[CrossRef](#)]
42. de Andrés-Toro, B.; Giron-Sierra, J.M.; Lopez-Orozco, J.A.; Fernandez-Conde, C.; Peinado, J. M.; García-Ochoa, F. Multiobjective optimization and multivariable control of the beer fermentation process with the use of evolutionary algorithms. *J. Zhejiang Univ. Sci.* **2004**, *5*, 378–389. [[CrossRef](#)]
43. Carrillo-Ureta, G.E.; Roberts, P.D.; Becerra, V.M. Genetic algorithms for optimal control of beer fermentation. In Proceedings of the 2001 IEEE International Symposium on Intelligent Control (ISIC'01), Mexico City, Mexico, 5–7 September 2001.
44. Saison, D. Effect of fermentation conditions on staling indicators in beer. *J. Am. Soc. Brew. Chem.* **2009**, *67*, 222–228. [[CrossRef](#)]
45. Buiatti, S. Beer composition: An overview. In *Beer in Health & Disease Prevention*; Elsevier: Amsterdam, The Netherlands, 2009; pp. 213–225.
46. Pires, E.J.; Teixeira, J.A.; Brányik, T. Yeast: The soul of beer's aroma—A review of flavour-active esters and higher alcohols produced by the brewing yeast. *Appl. Microbiol. Biotechnol.* **2014**, *98*, 1937–1949. [[CrossRef](#)] [[PubMed](#)]
47. Nelder, J.A.; Mead, R. A simplex method for function minimization. *Comput. J.* **1965**, *7*, 308–313. [[CrossRef](#)]
48. Angelopoulos, P.M.; Gerogiorgis, D.I.; Paspaliaris, I. Model-based sensitivity analysis and experimental investigation of perlite grain expansion in a vertical electrical furnace. *Ind. Eng. Chem. Res.* **2013**, *52*, 17953–17975. [[CrossRef](#)]
49. Biegler, L.T. *Nonlinear Programming: Theory, Algorithms, and Applications*; SIAM: Philadelphia, PA, USA, 2010.
50. NIST/SEMATECH. e-Handbook of Statistical Methods. Available online: <http://www.itl.nist.gov/div898/handbook/> (accessed on 1 May 2019).
51. Ivanov, K.; Petelkov, I.; Shopaska, V.; Denkova, R.; Gochev, V.; Kostov, G. Investigation of mashing regimes for low-alcohol beer production. *J. Inst. Brew.* **2016**, *122*, 508–516. [[CrossRef](#)]